

How does liquidity shape the yield curve?

Victor Le Coz,^{1,2,3,4,*} Iacopo Mastromatteo,^{5,†} and Michael Benzaquen^{1,2,5,‡}

¹*Chair of Econophysics and Complex Systems,
École polytechnique,
91128 Palaiseau Cedex,
France*

²*LadHyX UMR CNRS 7646,
École polytechnique,
91128 Palaiseau Cedex,
France*

³*Laboratoire de Mathématiques et Informatique pour la Complexité et les Systèmes,
CentraleSupélec, Université Paris-Saclay,
91192 Gif-sur-Yvette Cedex,
France*

⁴*Quant AI Lab, 29 Rue de Choiseul 75002 Paris,
France*

⁵*Capital Fund Management,
23 Rue de l'Université, 75007 Paris,
France*

(Dated: September 26, 2024)

The phenomenology of the forward rate curve (FRC) can be accurately understood by the fluctuations of a stiff elastic string (Le Coz and Bouchaud, 2024). By relating the exogenous shocks driving such fluctuations to the surprises in the order flows, we elevate the model from purely describing price variations to a microstructural model that incorporates the joint dynamics of prices and order flows, accounting for both impact and cross-impact effects. Remarkably, this framework allows for at least the same explanatory power as existing cross-impact models, while using significantly fewer parameters. In addition, our model generates liquidity-dependent correlations between the forward rate of one tenor and the order flow of another, consistent with recent empirical findings. We show that the model also account for the non-martingale behavior of prices at short timescales.

I. INTRODUCTION

A. Motivation

The forward interest rate $f(t, T)$, which will be defined more precisely further down, represents the interest rate agreed at time t for an instantaneous loan spanning from $T \geq t$ to $T + dT$. The collection of forward rates can be thought of as a continuous string that changes shape over time. An accurate understanding of the behavior of the forward interest rate curve (FRC) is essential in various fields, including interest rate derivative pricing and risk management (Hull, 2018; Brigo and Mercurio, 2006).

In an earlier article, J-P Bouchaud and one of the authors (VLC) revisited a model of the FRC based on the fluctuations of a stiff elastic string (henceforth called the BBDL model for *Baaquie-Bouchaud Discrete Logarithm* model (Le Coz and Bouchaud, 2024; Baaquie and Bouchaud, 2004)). Compared to previous work, this approach accounts for two important features: (a)

the discrete set of traded maturities, and (b) the scale-dependent structure of the correlation matrix across maturities (Epps, 1979).

The objective of this article is to demonstrate that this model can be given a microstructural interpretation, which allows for new predictions. Specifically, we establish a connection between a non-measurable auxiliary noise field that appears in the construction of the original model and the physically measurable volumes traded across the interest rates curve, thus promoting the string model (Le Coz and Bouchaud, 2024) to a microstructural model capable of predicting the price reaction to traded volumes along the curve. The resulting model is more parsimonious than other cross-impact models while maintaining comparable, if not superior, performance. We will show that it faithfully accounts for the effect of liquidity on the price-volume correlations between the forward rates of different maturities and the order flow (Le Coz *et al.*, 2024). Additionally, within this framework, prices appear to exhibit short-term temporal autocorrelations, consistent with established findings in the literature.

* victor.lecoz@gmail.com

† iacopo.mastromatteo@cfm.com

‡ michael.benzaquen@polytechnique.edu

B. Literature review

1. Arbitrage-free and field theories

Modeling of the forward interest rate curve has been predominantly influenced by the Heath-Jarrow-Morton framework since the 1990s (Heath *et al.*, 1992). This seminal theory posits a finite number of risk factors, which theoretically implies the existence of risk-free portfolio directions. Addressing this limitation, various researchers have ventured beyond the conventional boundary of a finite number of driving Brownian motions (Baaquie and Bouchaud, 2004; Kennedy, 1994, 1997; Goldstein, 2000; Santa-Clara and Sornette, 2001; Baaquie, 2001, 2002, 2004; Cont, 2005). In the following years, these random field theories have been applied to solve interest rate derivative pricing problems (Bueno-Guerrero *et al.*, 2015, 2016, 2020, 2022; Baaquie, 2007, 2009, 2010, 2018; Baaquie and Tang, 2012; Baaquie and Liang, 2007; Wu and Xu, 2014).

Elaborating on the work of (Baaquie and Bouchaud, 2004; Baaquie, 2001, 2002, 2004), Le Coz and Bouchaud (2024) have proposed a random field theory formulated on a discrete space of maturities. As previously mentioned, this approach closely reproduces the phenomenology of the FRC (Bouchaud *et al.*, 1999) and complies with the empirical finding of negligible correlation at small time scales (Epps, 1979).

2. Market micro-structure

Standard economic theory posits that an asset's price should reflect all publicly available information about its fundamental value. In reality, price formation occurs through a trading process in which information is gradually integrated into prices via the order flow of market participants. This widely recognized process is referred to as *price impact*. Kyle (1985) introduced an early model of price impact, assuming a linear relationship between absolute price differences and signed volumes traded. To reconcile the temporal autocorrelation of trades (Bouchaud *et al.*, 2018, 2004; Lillo and Farmer, 2004; Bouchaud *et al.*, 2009a; Yamamoto and LeBaron, 2010; Tóth *et al.*, 2015) with the temporal independence of price increments, Bouchaud *et al.* (2004) posited that price impact must decrease over time. This hypothesis has been confirmed by subsequent studies (Bouchaud *et al.*, 2006; Hopman, 2007; Bouchaud *et al.*, 2009b; Gatheral, 2010; Gatheral and Schied, 2013; Alfonsi *et al.*, 2016; Gârleanu and Pedersen, 2016; Tóth *et al.*, 2017; Taranto *et al.*, 2018; Ekren and Muhle-Karbe, 2019). This finding led to the formulation of the propagator model, where prices are expressed as the cumulative impact of all previous trades (Bouchaud *et al.*, 2018, 2006; Alfonsi *et al.*, 2016; Bouchaud, 2009; Benzaquen *et al.*,

2017; Schneider and Lillo, 2019).

A more subtle effect, known as *cross-impact*, occurs when the trading pressure in one asset influences the price of another. This phenomenon was initially studied by Hasbrouck and Seppi (2001) and later by Benzaquen *et al.* (2017); Schneider and Lillo (2019); Chordia *et al.* (2001); Evans and Lyons (2001); Harford and Kaul (2005); Pasquariello and Vega (2007); Andrade *et al.* (2008); Tookes (2008); Pasquariello and Vega (2015); Wang and Guhr (2017); Tomas *et al.* (2022a,b); Brigo *et al.* (2022). The simplest cross-impact models assume a linear relationship between signed trading volumes and price variations (Le Coz *et al.*, 2024; Hasbrouck and Seppi, 2001; Harford and Kaul, 2005; Pasquariello and Vega, 2007, 2015; Tomas *et al.*, 2022a,b). In particular, Le Coz *et al.* (2024) show that the interest rate curve exhibits significant cross-impact features. Bonds of different tenors are highly correlated and display a wide range of liquidity levels, which are the two characteristics required to accurately predict price changes using trading flows.

In addition, several authors (Bouchaud *et al.*, 2018, 2004; Plerou *et al.*, 2000; Cont, 2001; Elomari-Kessab *et al.*, 2024) have shown that price variations exhibit autocorrelation patterns over short timescales. These findings challenge the traditional viewpoint of market efficiency, which posits that price changes are memoryless.

Here we show that short-time-scale autocorrelation and cross-impact are compatible with the microfounded field theory of the FRC developed in Le Coz and Bouchaud (2024).

C. Definitions and notations

In this section, we define the forward interest rate and its signed order flow. Table II in appendix A provides a complete list of notations used in this article.

1. Forward interest rate

Let $P(t, T)$ denote the price at time t of a zero-coupon bond maturing at T . Such a bond pays one unit of currency at maturity T without any intermediate coupons. Consider time t and a future time T , where $t < T$. The instantaneous forward rate $f(t, T)$ is defined by

$$f(t, T) = -\frac{\partial \log P(t, T)}{\partial T}, \quad (1)$$

The collection of these rates for various T forms the forward interest rate curve.

In subsequent sections, we define the instantaneous forward rate $f(t, \theta)$ in terms of the time-to-maturity or *tenor* $\theta = T - t$. This dimension θ is often referred to as the *space* dimension, as opposed to the time dimension t .

2. Futures contracts

The instantaneous forward rate $f(t, \theta)$ is interpreted as the mid-price at time t of a 3-month SOFR Futures contract maturing at $t + \theta$. In practice, Futures contracts are available only for a discrete list of n tenors. In the following sections, we denote any process $x(t)$ defined in the discrete space of the existing tenors as a vector $(x_\theta(t))$. Therefore, we depart from the usual notation of the forward rate $f(t, \theta)$ to denote by $f_\theta(t)$ the closing forward rate of tenor θ in the time window $[t - \Delta t, t]$ with a length of $\Delta t = 1$ day. We then denote by $f(t) = (f_1(t), \dots, f_n(t))$ the column vector of the forward rates at closing, with the tenor θ in units of 3-months.

We define $\Delta q_\theta(t)$ as the net market order flow traded during the time window $[t - \Delta t, t]$ for the Future contract maturing in $t + \theta$. This is calculated by taking the sum of the volumes of all trades during that time period, with buy trades counted as positive and sell trades counted as negative. Thus, $\Delta q(t) = (\Delta q_1(t), \dots, \Delta q_n(t))$ is the column vector of net traded order flows.

3. Other notations

The set of real-valued square matrices of dimension n is denoted by $\mathbf{M}_n(\mathbb{R})$. Given A a positive symmetric matrix, we write $A^{1/2}$ for a matrix such that $A^{1/2}(A^{1/2})^\top = A$, and \sqrt{A} for the matrix square root: the unique positive semi-definite symmetric matrix such that $(\sqrt{A})^2 = A$. We also write $\text{diag}(A)$ for the vector in \mathbb{R}^n formed by the diagonal elements of A . Given a vector v in \mathbb{R}^n , we denote the components of v by (v_1, \dots, v_n) , and the diagonal matrix whose components are the components of v by $\text{diag}(v)$. We also define I_k with $k \in \llbracket -n, n \rrbracket$ as a matrix with ones only on the k -th diagonal above the main diagonal, i.e.,

$$(I_k)_{ij} = \begin{cases} 1 & \text{if } j - i = k, \\ 0 & \text{otherwise.} \end{cases} \quad (2)$$

Note that I_0 is the identity matrix simply denoted I .

II. A FIELD THEORY OF THE FRC

In this section, we summarize several results related to the correlated noise field developed in Le Coz and Bouchaud (2024). We also introduce some additional properties of such a noise field.

Let $\eta(t)$ denote a vector of independent Gaussian (Langevin) noises such that:

$$\mathbb{E}[\eta_\theta(t)\eta_{\theta'}(t')] = \delta(t - t')\delta_{\theta\theta'}, \quad (3)$$

where $\delta_{\theta\theta'}$ is the Kronecker delta, $\delta(\cdot)$ is the Dirac delta, and $\mathbb{E}[\cdot]$ denotes an unconditional expectancy. Note

that the vector of stochastic processes $B(t)$, defined by $dB(t) = \eta(t)dt$, represents a multidimensional Brownian motion.

The vector of the driftless discrete noise field $A(t)$ is defined for $\theta \in \llbracket 1, n \rrbracket$ as the solution to a differential equation which operates on a temporal scale $\tau \ll 1$ day:

$$\begin{cases} \frac{dA}{dt}(t) = \frac{1}{\tau} [-\mathcal{M}A(t) + \eta(t)], \\ A_1(t) - A_{-1}(t) = 0, \end{cases} \quad (4)$$

where \mathcal{M} is a matrix of $\mathbf{M}_n(\mathbb{R})$ defined by

$$\begin{aligned} \mathcal{M}_{\theta\theta'} &= 1 - \frac{1}{2\psi\mu^2} \left(1 + \frac{\theta}{\psi}\right) (I_1 - I_{-1})_{\theta\theta'} \\ &\quad - \frac{1}{\mu^2} \left(1 + \frac{\theta}{\psi}\right)^2 (I_1 - 2I + I_{-1})_{\theta\theta'}, \end{aligned} \quad (5)$$

with ψ the psychological time parameter and μ the line tension parameter (Le Coz and Bouchaud, 2024). Note that the boundary condition in Eq. (4) exhibits a term A_{-1} generated by the use of an Euler scheme centered in 0 to ensure the validity of the method of images used in Le Coz and Bouchaud (2024).

Here, we use a white noise $\eta(t)dt$ of variance dt instead of $2Ddt$ as in Le Coz and Bouchaud (2024); this choice has no impact on the results. Moreover, we consider a finite number n of diffusion factors, one for each tenor of the FRC, although the model could be written with an infinite-dimensional white noise η . In any case, only the first n component of the vector Y (see section III.B) would be non-zero.

Although Eq. (4) cannot be solved in closed form for arbitrary values of ψ , it simplifies in the two limits $\psi \rightarrow \infty$ and $\psi \rightarrow 0$. The general solution to Eq. (4) is expressed as

$$A(t) = \frac{1}{\tau} \int_{-\infty}^t dt' G(t - t') \eta(t'), \quad (6)$$

where the matrix $G(t - t')$ is the *propagator* of the noise $\eta(t')$. When $\psi \gg 1$, for $(\theta, \theta') \in \llbracket 1, n \rrbracket^2$, $G_{\theta\theta'}$ is given by (Le Coz and Bouchaud, 2024):

$$\begin{aligned} G_{\theta\theta'}(t) &:= \\ &\frac{1}{2\pi} \int_{-\pi}^{\pi} d\xi \left(e^{i\xi(\theta - \theta')} + e^{i\xi(\theta + \theta')} \right) e^{-\frac{L_d(\xi)}{\tau} t}, \end{aligned} \quad (7)$$

where $L_d(\xi) = 1 + 2\frac{(1 - \cos \xi)}{\mu^2}$. When $\psi \ll 1$, G becomes (Le Coz and Bouchaud, 2024):

$$G(t) := e^{-\frac{t}{\tau} \mathcal{M}} \mathcal{J}, \quad (8)$$

where \mathcal{J} denotes a diagonal matrix whose first entry is 2 and all other entries are 1. In this limit, the matrix \mathcal{M} can be written as a function of a single parameter $\kappa = \mu\psi$:

$$\mathcal{M}_{\theta\theta'} = I - \frac{\theta}{\kappa^2} (I_1 - I_{-1}) - \frac{\theta^2}{\kappa^2} (I_1 - 2I + I_{-1}). \quad (9)$$

A critical characteristic of the noise field $A(t, \theta)$ is its auto-covariance across time and space. For τ near 0, the auto-covariance of its integral over a time interval Δt , defined by $\Delta A := \int_{t-\Delta t}^t A_\theta(u) du$ is given by (Le Coz and Bouchaud, 2024):

$$\mathbb{E} [\Delta A(t) \Delta A^\top(t')] = \begin{cases} 0, & \text{if } |t - t'| > \Delta t, \\ \Delta t C, & \text{if } t = t', \end{cases} \quad (10)$$

where the matrix C is the *correlator* of ΔA . The latter is defined by (Le Coz and Bouchaud, 2024):

$$C := \begin{cases} \mathcal{D}_2 & \text{if } \psi \gg 1, \\ \mathcal{M}^{-1} \mathcal{J}^2 (\mathcal{M}^{-1})^\top & \text{if } \psi \ll 1, \end{cases} \quad (11)$$

where the matrix \mathcal{D}_k is given by

$$(\mathcal{D}_k)_{\theta\theta'} := \frac{1}{\pi} \int_0^\pi d\xi \frac{2 \cos \xi \theta \cos \xi \theta'}{L_d(\xi)^k}. \quad (12)$$

The second important property of the cumulative sum of A is its response to the generating white noise. We define the integrated η by $\Delta \eta_\theta(t) := \int_{t-\Delta t}^t \eta_\theta(u) du$. For τ near 0, the covariance between $\Delta A(t)$ and $\Delta \eta(t)$ reads

$$\mathbb{E} [\Delta A(t) \Delta \eta^\top(t)] = \Delta t R, \quad (13)$$

where the matrix R is the response of ΔA to $\Delta \eta$ given by:

$$R := \begin{cases} \mathcal{D}_1 & \text{if } \psi \gg 1, \\ \mathcal{M}^{-1} \mathcal{J} & \text{if } \psi \ll 1. \end{cases} \quad (14)$$

Hence, the correlation matrix $\rho(\Delta A(t), \Delta \eta(t))$ between $\Delta A(t)$ and $\Delta \eta(t)$ reads

$$\rho(\Delta A(t), \Delta \eta(t)) = \text{diag}(\sigma_A)^{-1} R, \quad (15)$$

where σ_A is the volatility vector of ΔA defined by

$$(\sigma_A)_\theta = \sqrt{\text{diag}(C)_\theta}. \quad (16)$$

The proofs of these properties are provided in appendices B and C.

The noise field A is now employed to model forward rates. The diffusion equation for the variations of the forward rate, denoted as $df_\theta(t)$, is given by (Le Coz and Bouchaud, 2024):

$$\frac{df}{dt}(t) = \text{diag}(\sigma) \text{diag}(\sigma_A)^{-1} A(t), \quad (17)$$

where the component σ_θ of the vector σ is the volatility of the noise term driving the forward rate f_θ . Hence, the equal-time Pearson correlation coefficient among coarse-grained forward rate variations $\Delta f := \int_{t-\Delta t}^t df(u)$ is given by (Le Coz and Bouchaud, 2024):

$$\rho(\Delta f, \Delta f) = \text{diag}(\sigma_A)^{-1} C \text{diag}(\sigma_A)^{-1}. \quad (18)$$

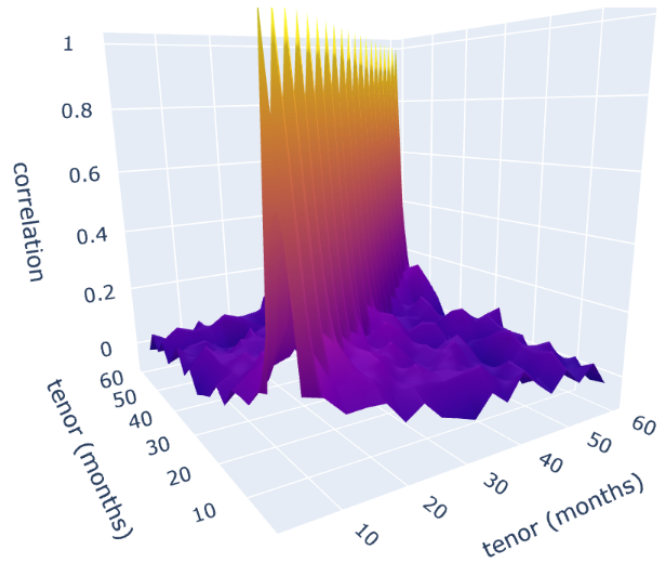


FIG. 1: Spatial Pearson correlations of the signed daily order flows of SOFR Futures from 2016 to 2023.

III. TOWARDS A CROSS-IMPACT MODEL

Although the model of Le Coz and Bouchaud (2024) provides an accurate account of the correlation structure of the FRC, it does not clarify the nature of the exogenous noise η driving the dynamics of the curve. In this section we want to provide a microstructural foundation for the η noise by linking it to the surprise in the order flow, thus promoting the model (that only describes price variations) to a microstructural model accounting for the joint dynamics of prices and volumes.

A. Order flow decomposition

Trading flows exhibit significantly lower spatial correlation compared to prices, as shown in Fig. 1. However, they display long range temporal autocorrelation (see Bouchaud *et al.* (2018) and the literature mentioned in section I.B.2). Therefore, we provide a natural physical interpretation of the white noise η by assuming that this noise corresponds to the surprise (i.e. the martingale component) in the signed order flow. However, only a fraction of the volatility of price increments is expected to be explained by trades (see section VI), so the white noise column vector $\eta(t)$ is decomposed into an idiosyncratic component η^\perp , and a component related to order flow η^q :

$$\eta(t) = \text{diag}(Y) \eta^q(t) + \text{diag}(Y^\perp) \eta^\perp(t), \quad (19)$$

where η^\perp is a normalized white noise independent from η^q and Y is the vector of the parameters $Y_\theta \in [0, 1]$ governing, for each tenor θ , the share of forward rates vari-

ance explained by the order flow imbalance. The components of the vector Y^\perp are $Y_\theta^\perp = \sqrt{1 - Y_\theta^2}$. Formally, the surprise $\eta^q(t)$ is defined as

$$\eta^q(t) := O \int_{-\infty}^t dt' J(t-t') \frac{dq}{dt}(t'), \quad (20)$$

where $\frac{dq}{dt}(t')$ is the infinitesimal order flow imbalance, and $J(t-t')$ is a matrix-valued function that ensures the diffusivity of the process $\eta^q(t)$, i.e., $\mathbb{E}[\eta_\theta^q(t)\eta_{\theta'}^q(t')] = \delta_{\theta\theta'}\delta(t-t')$. Such an operator is defined up to an arbitrary rotation matrix O which leaves the price process invariant.

In appendix D, we justify the existence of the kernel J in Eq. (20), assuming the lagged variance-covariance matrix of the infinitesimal order flows $\Omega(t, t') := \mathbb{E}\left[\frac{dq}{dt}(t)\frac{dq}{dt}^\top(t')\right]$ is stationary: $\Omega(t, t') = \Omega(t-t')$. We further assume that the order flow has a factorized structure¹

$$\Omega(t-t') = \text{diag}(\phi(t-t'))\Omega, \quad (21)$$

where the function $\ell \mapsto \phi(\ell)$ is valued in vector space, and Ω is the equal-time variance-covariance matrix of the infinitesimal order flows. Then, it is quite simple to obtain an explicit expression for $J(t-t')$ (see appendix D):

$$J(t-t') = \Omega^{-1/2} \text{diag}(\Phi(t-t')), \quad (22)$$

where $\Phi(\ell)$ is an operator, valued in vector space, denoting the element-wise convolutional inverse of $\phi(\ell)$.

Note that this construction leaves the rotation matrix O undefined. In section III.D, we propose a method to determine this matrix to satisfy the consistency requirements of a cross-impact model.

Finally, one can define $\tilde{q}(t)$, the martingale component of $q(t)$, through:

$$\frac{d\tilde{q}}{dt}(t) := \int_{-\infty}^t dt' \text{diag}(\Phi(t-t')) \frac{dq}{dt}(t'), \quad (23)$$

such that the surprise η^q is given by

$$\eta^q(t) = O\Omega^{-1/2} \frac{d\tilde{q}}{dt}(t). \quad (24)$$

B. Noise field decomposition

The decomposition of the white noise η enables us to write the noise field A as the sum of two independent components:

$$A(t) = A^q(t) + A^\perp(t), \quad (25)$$

where the correlated noise A^q is the solution of

$$\begin{cases} \frac{dA^q}{dt}(t) = \frac{1}{\tau} [-\mathcal{M}A^q(t) + \text{diag}(Y)\eta^q(t)], \\ A_1^q(t) - A_{-1}^q(t) = 0. \end{cases} \quad (26)$$

The correlated noise A^\perp solves a similar equation with the generating white noise $\text{diag}(Y^\perp)\eta^\perp(t)$.

C. Large-bin approximation

Even though Eq. (6) shows that $\Delta A(t)$ depends upon the whole history of $\eta(t')$ for $t' \leq t$, we are interested in approximating $\Delta A_\theta(t)$ as a function of coarse-grained variables $\Delta\eta$ defined over intervals of finite width Δt , as in practice we will have empirical access to order flows sampled on a discrete time grid. The proofs of the results presented in this section are detailed in appendix E.

We decompose the white noise column vector $\eta(t')$ into the sum of its observed empirical averages over the time intervals $[t-\Delta t, t]$ (i.e. its moving average) and its fluctuations around this mean. Formally, we write

$$\eta(t') = \bar{\eta}_{\Delta t}(t) + \eta(t') - \bar{\eta}_{\Delta t}(t), \quad (27)$$

where $\bar{\eta}_{\Delta t}(t)$ is the empirical mean of $\eta(t)$ over the time window $[t-\Delta t, t]$ i.e.,

$$\bar{\eta}_{\Delta t}(t) := \frac{1}{\Delta t} \int_{t-\Delta t}^t dt' \eta(t'). \quad (28)$$

If we further consider that $\tau \ll \Delta t$ one can express $\Delta A_\theta(t)$ as a function of $\bar{\eta}_{\Delta t}(t)$:

$$\Delta A(t) = R \Delta t \bar{\eta}_{\Delta t}(t) + \int_{t-\Delta t}^t dt' \epsilon^\tau(t'), \quad (29)$$

where $\epsilon^\tau(t) = \frac{1}{\tau} \int_{t-\Delta t}^t dt' G(t-t') (\eta(t') - \bar{\eta}_{\Delta t}(t))$ is a noise independent of $\bar{\eta}_{\Delta t}(t)$ (see appendix E). One can substitute η with η^q or η^\perp and A with A^q or A^\perp in Eq. (29). It yields a relationship between forward rate daily increments and the martingale component of the daily order flow $\Delta\tilde{q}(t) := \int_{t-\Delta t}^t dt' \tilde{q}(t')$:

$$\widehat{\Delta f}(t) = \text{diag}(\sigma) \text{diag}(\sigma_A)^{-1} R \text{diag}(Y) O \Omega^{-1/2} \Delta\tilde{q}(t), \quad (30)$$

where $\widehat{\Delta f}$ denotes the conditional expectancy of the forward rates increments Δf with respect to these flows:

$$\widehat{\Delta f}(t) := \mathbb{E}[\Delta f(t) | \Delta\tilde{q}(t)]. \quad (31)$$

Similarly to the approach of Le Coz *et al.* (2024), we neglect the autocorrelation of the order flows, such that $\Delta\tilde{q}(t) \approx \Delta q(t)$. This approximation is adequate on the daily time scale for 80% of the maturities considered in our sample (see Fig. 2). Hence, one can write the condi-

¹ Even though this assumption is not strictly required in our construction, we prefer to stick to this simpler case, which is an acceptable first order approximation of the empirical order flow structure, see (Benzzaquen *et al.*, 2016).

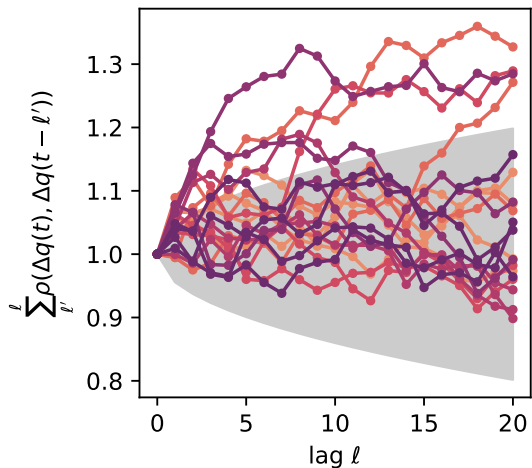


FIG. 2: Accumulated temporal autocorrelation of daily trading flows over ℓ days i.e., $\sum_{\ell'}^{\ell} \rho(\Delta q(t), \Delta q(t - \ell'))$. Each color corresponds to the tenor of a SOFR Future contract ranging from 3 to 60 months over the period 2016 – 2023. Only 4 maturities (15, 21, 27 and 45 months) out-of-20 are outside the confidence interval after 20 days.

tional expectancy of the forward rates daily increments with respect to the order flow as

$$\widehat{\Delta f}(t) = \text{diag}(\sigma) \text{diag}(\sigma_A)^{-1} R \text{diag}(Y) O \Omega^{-1/2} \Delta q(t). \quad (32)$$

D. Cross-impact matrix

Equation (32) can be used to define a cross-impact model. Let $\Lambda \in \mathbf{M}_n(\mathbb{R})$ be the matrix such that the equal-bin linear relationship between forward rates increments and order flows reads

$$\Delta f(t) = \Lambda \Delta q(t) + \mathcal{E}(t), \quad (33)$$

where \mathcal{E} is a temporally uncorrelated noise independent from Δq . Identifying Λ in Eq. (32) yields

$$\Lambda = \text{diag}(\sigma) \text{diag}(\sigma_A)^{-1} R \text{diag}(Y) O \Omega^{-1/2}. \quad (34)$$

This formula can also be derived by computing Λ as the linear response of the forward rates to the equal-time order-flow:

$$\Lambda := \mathbb{E} [\Delta f(t) \Delta q(t)^\top] \mathbb{E} [\Delta q(t) \Delta q(t)^\top]^{-1}. \quad (35)$$

The proof of this alternative approach is provided in appendix F. In addition, appendix G shows that the correlation between the forward rate and the order flow is well defined.

The cross-impact model in Eq. (34) is fully determined up to an arbitrary rotation matrix O . This free parameter can be used to ensure that our model has the required (i) rotational invariance, (ii) non-arbitrage, (iii) fragmentation invariance, and (iv) stability properties (Tomas *et al.*, 2022b). In fact, it was shown that the cross-impact matrix Λ that satisfies these properties must be symmetric positive definite (Tomas *et al.*, 2022b). The rotation O_{sym} ensuring that Λ fulfills these properties is given by (del Molino *et al.*, 2020):

$$O_{\text{sym}}(M, \Omega^{1/2}) := M^{-1} (\Omega^{-1/2})^\top \sqrt{(\Omega^{1/2})^\top M M^\top \Omega^{1/2}}, \quad (36)$$

where $M = \text{diag}(\sigma) \text{diag}(\sigma_A)^{-1} R \text{diag}(Y)$.

As an alternative model that does not meet these constraints, one can also simply choose $O = I$ the identity matrix. We will refer to the cross-impact model using Eq. (34) as BBDLW for Baaquie-Bouchaud Discrete Logarithm Whitening when $O = I$ and BBDLS for Baaquie-Bouchaud Discrete Logarithm Symmetric when $O = O_{\text{sym}}$.

IV. CALIBRATION

The best empirical fits of the BB model are obtained in the limit $\psi \rightarrow 0$ (see Le Coz and Bouchaud (2024)), which is therefore chosen for calibration.

Our data set comprises historical daily price variations and net market order flows of SOFR Futures contracts from July 2015 to 2023. We observe $n = 20$ different tenors ranging from 3 to 60 months. 3-month SOFR Futures contracts were not available before March 2022; thus, Eurodollar contracts were used before that time, with an appropriate three-month shift accounting for the forward-looking nature of the Eurodollar Futures as opposed to the backward-accrued SOFR.

A. Methodology

In line with the approach of Le Coz and Bouchaud (2024), we fit the parameter κ in formula (18) to the observed forward rate correlation matrix within our dataset segmented into 3 periods: 2015 – 2017, 2018 – 2020 and 2021 – 2023. In addition, we fit the vector Y by minimizing the square differences between the daily increments of modeled forward rates, $\widehat{\Delta f}$, and the empirical ones, Δf , using Eq. (32).

To overcome the conditional heteroskedasticity of forward rate variations, we use a daily estimator of their volatility. Let $\{t_1, \dots, t_N\}$ denote the N business days of a period of 3 years. For each day t_k , the estimators of the forward rates increments and order flow's volatility

are defined by

$$\begin{aligned}\widehat{\sigma}^2(t_k) &:= (\langle \Delta f_1(t)^2 \rangle(t_k), \dots, \langle \Delta f_n(t)^2 \rangle(t_k)), \\ \widehat{\omega}^2(t_k) &:= (\langle \Delta q_1(t)^2 \rangle(t_k), \dots, \langle \Delta q_n(t)^2 \rangle(t_k)),\end{aligned}\quad (37)$$

where the operator $\langle \cdot \rangle(t_k)$ denotes the moving-average computed using the last 20 daily data points before the day t_k . We assume the order flow correlation matrix $\text{diag}(\omega(t))^{-1} \Omega(t) \text{diag}(\omega(t))^{-1}$ is stationary. Let $\widehat{\rho}(\Delta q, \Delta q)$ denote its canonical empirical estimator using 3 years of data. On day t_k , the estimated variance-covariance matrix $\widehat{\Omega}(t_k)$ is computed as

$$\widehat{\Omega}(t_k) := \text{diag}(\widehat{\omega}(t_k)) \widehat{\rho}(\Delta q, \Delta q) \text{diag}(\widehat{\omega}(t_k)). \quad (38)$$

We define similarly the estimated variance-covariance of the forward rate variations and the estimated response matrices as

$$\begin{aligned}\widehat{\Sigma}(t_k) &:= \text{diag}(\widehat{\sigma}(t_k)) \widehat{\rho}(\Delta f, \Delta f) \text{diag}(\widehat{\sigma}(t_k)), \\ \widehat{R}(t_k) &:= \text{diag}(\widehat{\sigma}(t_k)) \widehat{\rho}(\Delta f, \Delta q) \text{diag}(\widehat{\omega}(t_k)).\end{aligned}\quad (39)$$

The predicted forward rate change on day t_k is defined as

$$\widehat{\Delta f}(t_k) = \widehat{\Lambda}^{\text{model}}(t_k) \Delta q(t_k), \quad (40)$$

where $\widehat{\Lambda}^{\text{model}}(t_k)$ is the cross-impact matrix estimated on day t_k in the tested model.

In the case of our noise field approach, the cross-impact matrix is given by

$$\widehat{\Lambda}^{\text{BB}}(t_k) = \text{diag}(\widehat{\sigma}(t_k)) \text{diag}(\sigma_A)^{-1} R \text{diag}(Y) O \widehat{\Omega}(t_k)^{-1/2}, \quad (41)$$

where $O = O_{\text{sym}}$ or $O = I$ depending on the tested model.

In order to compare the results of our model with other cross-impact models, we define three other cross-impact matrices (studied, for example, in Le Coz *et al.* (2024)). Let y denote a scalar called the Y-ratio. We consider:

- the diagonal model, defined by

$$\widehat{\Lambda}^{\text{diag}}(t_k) := y \text{diag}(\widehat{R}(t_k)) \text{diag}(\widehat{\Omega}(t_k)^{-1}), \quad (42)$$

which is the limit case where the cross-sectional impact is set to zero;

- the Maximum Likelihood model (ML model in the following sections), defined by

$$\widehat{\Lambda}^{\text{ML}}(t_k) := y \widehat{R}(t_k) \widehat{\Omega}(t_k)^{-1}; \quad (43)$$

- and the so-called Kyle model, defined by

$$\begin{aligned}\widehat{\Lambda}^{\text{Kyle}}(t_k) &:= \\ &y \widehat{\Sigma}(t_k)^{1/2} O_{\text{sym}} \left(\widehat{\Sigma}(t_k)^{1/2}, \widehat{\Omega}(t_k)^{1/2} \right) \widehat{\Omega}(t_k)^{-1/2}.\end{aligned}\quad (44)$$

The ML model does not impose any constraints on the cross-impact model, so it generates the best possible in-sample fit. The Kyle model ensures (i) rotational invariance, (ii) non-arbitrage, (iii) fragmentation invariance, and (iv) stability properties (Tomas *et al.*, 2022b; del Molino *et al.*, 2020). However, none of these models prescribes the form of the price variance-covariance matrix. Such a matrix is fully determined within the BBDL model thanks to a single parameter κ in the case $\psi \ll 1$ (see section II).

B. Goodness-of-fit

To assess the model goodness-of-fit, we compare the predicted price changes $\widehat{\Delta f}(t)$ with the realized price changes $\Delta f(t)$. For this evaluation, we employ a generalized R-squared, parameterized by a symmetric, positive matrix W . The W -weighted generalized $\mathcal{R}^2(W)$ is given by

$$\begin{aligned}\mathcal{R}^2(W) &:= \\ &1 - \frac{\sum_{k=1}^N (\Delta f(t_k) - \widehat{\Delta f}(t_k))^\top W(t_k) (\Delta f(t_k) - \widehat{\Delta f}(t_k))}{\sum_{k=1}^N \Delta f(t_k)^\top W(t_k) \Delta f(t_k)}.\end{aligned}\quad (45)$$

The closer this score is to one, the better the fit to actual prices. To highlight different sources of error, different choices of W can be considered:

- $W_\sigma(t) := \text{diag}(\widehat{\sigma}^2(t))^{-1}$, to account for errors relative to the typical deviation of the assets considered. This type of error is relevant for strategies that predict idiosyncratic moves of the constituents of the basket, rather than strategies that wager on correlated market moves.
- $W_{\sigma_\theta}(t) := \text{diag}((0, \dots, 0, \widehat{\sigma}_\theta^2(t), 0, \dots, 0))^{-1}$, to account for the errors of a single asset θ .

The weights W_σ are used in section IV.C to compare the overall performance of cross-impact models, while the weights $W_{\sigma_\theta}(t)$ are used in section VI to measure their properties in a pairwise setting.

C. Results

The results of the calibration of the BBDL model on empirical correlations of the forward rate are presented in table I. This confirms the high accuracy and good parameter stability of the BBDL model.

Using the calibrated line tension parameter κ reported in table I, we fit the share of explained volatility Y to the time series of rates and order flows of SOFR Futures. The calibrated share Y of the explained forward rate volatility

Period	κ	\mathcal{R}^2
2015–2017	0.84	99.9%
2018–2020	0.82	99.4%
2021–2023	1.3	97.1%

TABLE I: Calibrated line tension parameter κ in the BBDL model for each 3-year period in our sample. Here, \mathcal{R}^2 denotes the share of the explained variance of the empirical correlations among forward rates of time-to-maturity ranging from 3 to 60 months.

is reported for each period in Fig. 3². It shows that the most liquid products (the shortest time-to-maturity θ) are associated with the highest values of Y_θ . We also observe that building the symmetric cross-impact model BBDLS requires setting the less liquid maturities of Y to zero (see Fig. 3) in order to avoid instabilities. One could improve the R-squared by putting more weight on the non-liquid products, but this would compromise the model’s no-arbitrage property.

The in-sample R-squared values reported in Fig. 4 show that, as expected, the BBDLW model performs worse than the unconstrained ML model, whereas the out-of-sample results show that the two models have similar performances. It is noteworthy because the BBDLW model uses only $n + 1$ parameters (excluding the parameters used for the whitening of the correlation matrix), while the ML model requires calibrating n^2 parameters. Furthermore, the BBDLS model is actually at least as accurate as the Kyle model in predicting forward rate moves. Once again, this is remarkable because the BBDLS model is more parsimonious than the Kyle model, which uses $\frac{n(n+1)}{2}$ parameters. In fact, the Kyle model, which features a unique Y -ratio for all assets, cannot explore the regime probed by BBDLS.

As expected, compared to the less constrained approaches (ML and BBDLW), the symmetrical models (Kyle and BBDLS) perform poorly in-sample (see Fig. 4). However, the out-of-sample results favor these symmetrical models, demonstrating that the market does not feature arbitrage opportunities large enough to rule out those models.

Using this set of calibrated parameters, one can draw the response of the forward rate curve to a trade with a notional value of one billion dollars in a single maturity

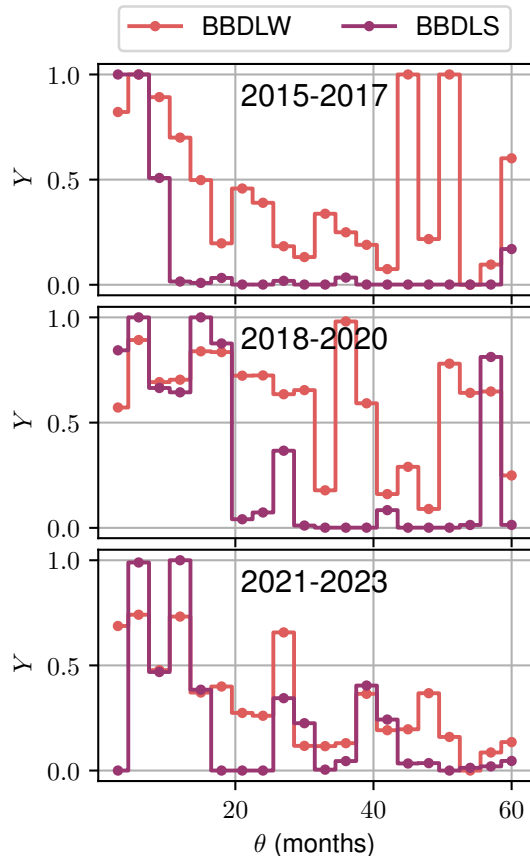


FIG. 3: Optimal parameters Y_θ governing the share of forward rates variances explained by order flows for each maturity θ .

over the course of one day. As our cross-impact models are re-scaled everyday by the daily volatility of prices and order flows (see section IV.A), Fig. 5 presents one column of the matrix Λ on a randomly chosen day within each three-year period. It shows that all models except the ML model predict a high price impact for the tenor being bought (in this case, 21 months).

V. NON-MARTINGALITY AT SMALL TIME-SCALES

Several authors have shown that price variations exhibit autocorrelation patterns over short time intervals (see the literature cited in section I.B.2). Our model is compatible with these results because, for time-scales $dt \leq \tau$ the forward rate process is not yet a martingale.

To illustrate this phenomenon, we assume that a volume V of the SOFR Future of time-to-maturity θ_0 is purchased during the time interval dt . Our goal is to calculate the progressive deformation of the FRC in response to this single trade. Formally, we define $d\tilde{q}(0) = V_{\theta_0}$, where $V_{\theta_0} = (0, \dots, 0, V, 0, \dots, 0)$ is a vector with a single

² More precisely, this calibration is performed by assuming $Y \in [0, 1]$ and calibrating the prices of SOFR Futures $p(t, \theta) = 100 - f(t, \theta)$ to the signed order flow. If we relax this constraint, the search for values $Y \in [-1, 1]$ also yields (almost) systematically positive coefficients because of the well-documented positive correlation between order flow and prices (Le Coz *et al.*, 2024). Indeed, across all periods and maturities (60 calibrated coefficients), we observe only 2 parameters Y_θ with slightly negative values (around -0.1).

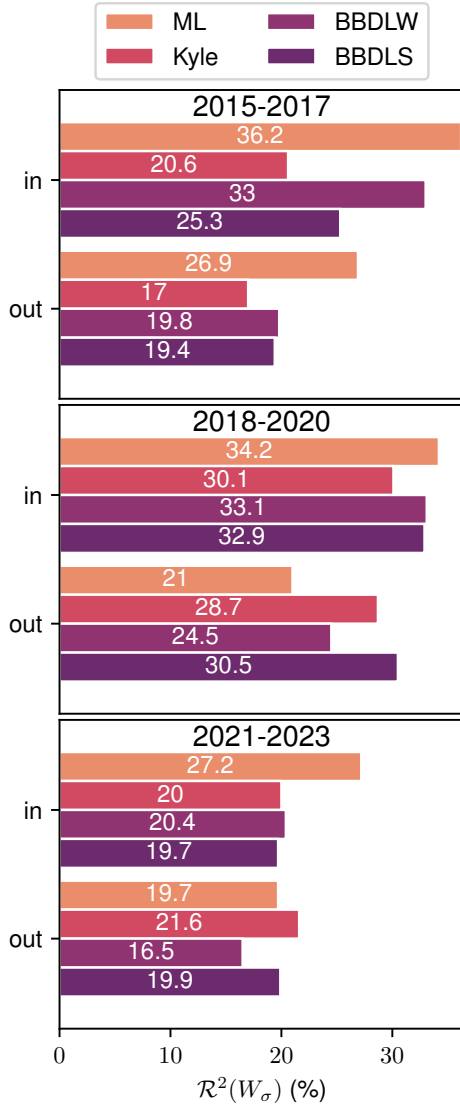


FIG. 4: Generalized R-squared $\mathcal{R}^2(W_\sigma)$ values both in- and out-sample for each period and model. The out-sample values are derived using the parameters calibrated from the preceding period. For the first period 2015 – 2017, the out-sample R-squared values are calculated using the parameters calibrated from the 2021 – 2023 period.

non-zero component V in the position θ_0 and $d\tilde{q}(t) = 0$ for $t > 0$. We now discretize time in Eqs (4), (17), (24), and (26). This yields an expression for the forward rate variations df at discrete times kdt in response to this single transaction:

$$df(kdt) = d\hat{f}(kdt) + \epsilon'(kdt). \quad (46)$$

Here, $\epsilon'(kdt)$ is a noise independent from the forward rate variations caused by trading activity $d\hat{f}(kdt)$, which

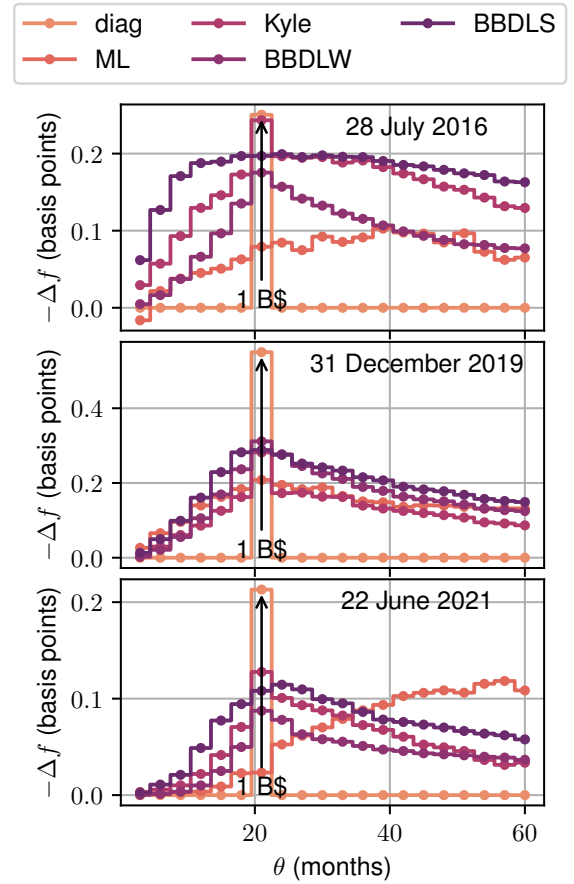


FIG. 5: Modeled FRC moves in response to a trade in the SOFR Future of maturity 21 months with a notional value of one billion dollars over the course of one randomly chosen day for each of the three calibration periods.

is defined as $d\hat{f}(kdt) :=$

$$\frac{1}{\tau} \text{diag}(\sigma) \text{diag}(\sigma_A)^{-1} \left(I - \frac{dt}{\tau} \mathcal{M} \right)^k \text{diag}(Y) \Omega^{-1/2} V_{\theta_0}. \quad (47)$$

Fig. 6 shows the predicted FRC responses to a transaction of volume $V = 1$ billion dollars in the 24-month Future occurring between $t = 0$ and $t = 0.25\% \times \tau$. Immediately following the trade, the price impact peaks at the traded maturity. The effect of this trade on the other tenors progressively spreads up to 3τ , where it becomes negligible. Based on the calibration by Le Coz and Bouchaud (2024), $\tau \approx 30$ minutes. Thus, Fig. 6 represents the resulting deformation of the FRC between 5 seconds and 1.5 hours after the trade.

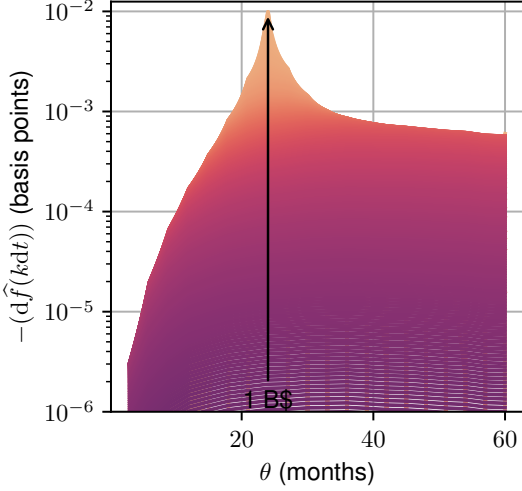


FIG. 6: FRC moves in the BBDLW model in response to a trade in the SOFR Future of maturity 24 months with a notional value of one billion dollars executed at time $t = 0$. Each color corresponds to a time step ordered from $t = 0.25\% \times \tau$ (orange) to 3τ (purple). The total response $\Delta \hat{f}$ over the time interval $\Delta t = 3\tau$ is the sum of all the infinitesimal responses $df(kdt)$.

VI. INFLUENCE OF LIQUIDITY ON PRICE-VOLUME CORRELATIONS

We now focus on the pair of assets with tenors θ and θ' . Our aim is to measure the degree to which the goodness-of-fit on the forward rate θ in a linear cross-impact model results from the order flow at θ' . For this purpose, we define the accuracy increase of cross-sectional information as

$$\Delta \mathcal{R}_{\theta' \rightarrow \theta}^{2, \text{model}} := \mathcal{R}^{2, \text{model}}(W_{\sigma_\theta}) - \mathcal{R}^{2, \text{diag}}(W_{\sigma_\theta}), \quad (48)$$

where the R-squared values are computed in a two-asset model. Le Coz *et al.* (2024) established that the price-volume correlation between different US sovereign bonds depends on the respective liquidity of the considered assets. Formally Le Coz *et al.* (2024) derive these results by observing that the pairwise additional R squared $\Delta \mathcal{R}_{\theta' \rightarrow \theta}^2$ obtained by the regression of a bond price on the order flow of another bond is highly asymmetrical. We reproduce these results for SOFR Futures contracts in Fig. 7. The vertical stripes show the effect of the liquidity of each asset on the price-volume correlation. In fact, in a 2-asset framework, the additional R-squared $\Delta \mathcal{R}_{\theta' \rightarrow \theta}^2$ is roughly equivalent to the squared price-volume correlation $\rho^2(\Delta f_\theta, \Delta q_{\theta'})$, due to the low spatial correlation of the order flow (see Fig. 1 and section VI.A).

In this section, we demonstrate that the BBDLW and BBDLS models capture this stylized fact, primarily due to the vector Y , which represents the share of price volatility attributable to trades. These liquidity-

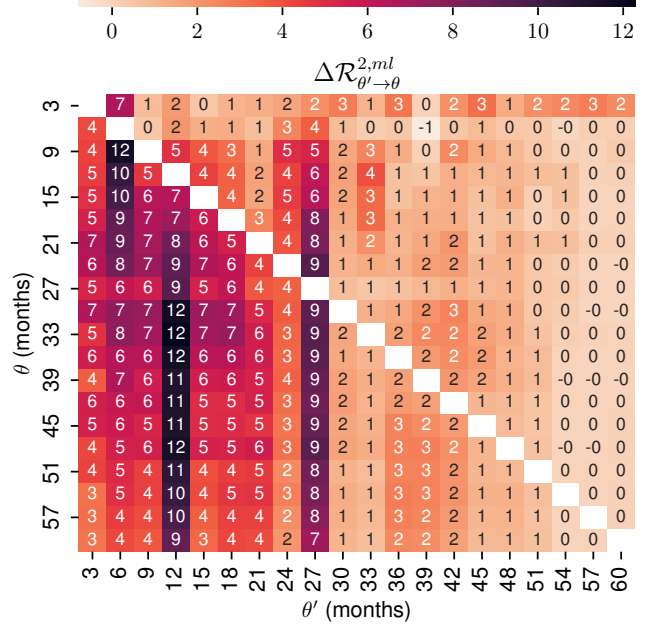


FIG. 7: Empirical added accuracy $\Delta \mathcal{R}_{\theta' \rightarrow \theta}^2$ when regressing daily forward rate increments of tenor θ on the order flows of tenor θ and θ' instead of solely on its own order flow, for the period 2021 – 2023. The calibration methodology is described in section IV.A.

dependent responses are neither replicated by the Kyle model (see section VI.B) nor by the noise fields A and η (see section VI.C), highlighting the significance of the parameter vector Y .

A. Theoretical ML model

In a two-asset ML model, the R-squared obtained from regressing the prices of the first asset to the order flow imbalance of the both assets is given by

$$\mathcal{R}^{2, \text{ML}}(W_{\sigma_1}) = \frac{1}{1 - \rho^2(\Delta q_1, \Delta q_2)} [\rho^2(\Delta f_1, \Delta q_1) + \rho^2(\Delta f_1, \Delta q_2) - 2\rho(\Delta q_1, \Delta q_2)\rho(\Delta f_1, \Delta q_1)\rho(\Delta f_1, \Delta q_2)], \quad (49)$$

where Δp_i and Δq_i are respectively the price increments and the order flow of assets $i \in \llbracket 1, 2 \rrbracket$. If one subtracts from the previous quantity the R-squared obtained when regressing the first asset prices on its own trading flow, one gets the theoretical added accuracy $\Delta \mathcal{R}_{2 \rightarrow 1}^{2, \text{ML}}$ in the ML model when regressing asset 1's prices on the order

flow imbalance of assets 1 and 2 instead of solely asset 2:

$$\begin{aligned}\Delta\mathcal{R}_{2\rightarrow 1}^{2,\text{ML}} &= \mathcal{R}_{2\rightarrow 1}^{2,\text{ML}}(W_{\sigma_1}) - \rho^2(\Delta f_1, \Delta q_1) \\ &= \frac{(\rho(\Delta f_1, \Delta q_2) - \rho(\Delta q_1, \Delta q_2)\rho(\Delta f_1, \Delta q_1))^2}{1 - \rho^2(\Delta q_1, \Delta q_2)}.\end{aligned}\quad (50)$$

Equation (50) indicates that $\Delta\mathcal{R}_{2\rightarrow 1}^{2,\text{ML}}$ depends solely on price and order flow correlations. A priori $\Delta\mathcal{R}_{2\rightarrow 1}^{2,\text{ML}}$ should be independent of the respective liquidity (i.e., the product $\sigma_i \times \omega_i$, where σ_i is the volatility of prices and ω_i the volatility of the order flow imbalance) of each asset. In fact, Fig. 1 illustrates that these R-squared values vary significantly across assets, suggesting that price-volume correlations are influenced by the liquidity of the assets in question (see Le Coz *et al.* (2024) for a detailed analysis of liquidity's effect on cross-impact).

B. Theoretical Kyle model

A numerical simulation clearly demonstrates the effect of liquidity in the Kyle model. Figure 8 shows the added precision $\Delta\mathcal{R}_{2\rightarrow 1}^{2,\text{Kyle}}$ in the Kyle model, when regressing the prices of the asset 1 on the order flow imbalance of the assets 1 and 2 instead of solely on the asset 2. Each pair of assets is identified by the liquidity $\sigma_i\omega_i$ of its individual assets. We assume that the Y-ratio remains constant for all pairs considered and $y = \rho(\Delta f_1, \Delta q_1)$. In other words, the Y-ratio is precisely equal to the correlation between price and volume for the explained asset. Figure 8 shows that, in this scenario, $\Delta\mathcal{R}_{2\rightarrow 1}^{2,\text{Kyle}}$ is close to zero for all the liquidity levels tested. This means that the Kyle model consistently generates an R-squared $\mathcal{R}_{2\rightarrow 1}^{2,\text{Kyle}}(W_\sigma)$ close to y^2 . It yields another interpretation of the Y-ratio in the Kyle model as the average effective correlation between prices and volumes.

C. Theoretical BBDL models

a. Responses of A to η . We first study the response of the correlated field A to its generating white noise η given by Eq. (15). Figure 9 shows the squared correlation between $\Delta A_\theta(t)$ and $\Delta\eta_{\theta'}(t)$ for a typical value of the calibrated parameter κ . This quantity represents the additional R squared from the regression of $\Delta A_\theta(t)$ to $\Delta\eta_{\theta'}(t)$ and $\Delta\eta_\theta(t)$ instead of only $\Delta\eta_\theta(t)$. Indeed, as $\Delta\eta_\theta(t)$ is independent from $\Delta\eta_{\theta'}(t)$ we have

$$\Delta\mathcal{R}_{\theta'\rightarrow\theta}^2 = \frac{\mathbb{E}[\Delta A_\theta(t)\Delta\eta_{\theta'}(t)]^2}{\mathbb{E}[\Delta A_\theta(t)^2]\mathbb{E}[\Delta\eta_{\theta'}(t)^2]} = \frac{R_{\theta\theta'}}{(\sigma_A)_\theta}.\quad (51)$$

Figure 9 shows that the correlation between noise A and its generating white noise η is asymmetrical and decreases with distance $|\theta - \theta'|$. This asymmetry arises from the rescaling by the norm σ_A of the noise field A , which

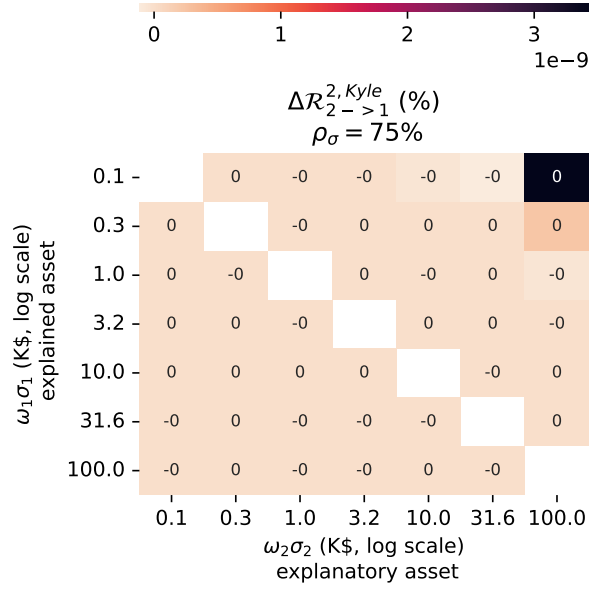


FIG. 8: Theoretical added accuracy $\Delta\mathcal{R}_{2\rightarrow 1}^{2,\text{Kyle}}$ in the Kyle model, when regressing the price of asset 1 on the order flow imbalance of assets 1 and 2 instead of solely asset 2. $\Delta\mathcal{R}_{2\rightarrow 1}^{2,\text{Kyle}}$ is represented as a function of the individual risk levels of each asset. The correlation between the order flows of assets 1 and 2 is $\rho_\omega = 50\%$. The correlation between the prices of assets 1 and 2 is $\rho_\sigma = 75\%$. The volatility of prices and volumes is defined as the square root of the risk level:

$$\sigma_1 = \omega_1 = \sqrt{\sigma_1\omega_1}.$$

decreases when θ increases. This decreasing volatility is an effect of psychological time: the higher the maturity, the shorter the distance between the nearby tenors; thus, the lower the volatility of each noise $A_{\theta'}$ generated from the normalized white noise η_θ .

b. Responses of the forward rate to η . In the BBDLW model, the additional R-squared from regressing $\Delta f_\theta(t)$ on $\Delta\eta_{\theta'}^q(t)$ and $\Delta\eta_\theta^q(t)$ instead of solely $\Delta\eta_\theta^q(t)$ is given by

$$\Delta\mathcal{R}_{\theta'\rightarrow\theta}^2 = \frac{\mathbb{E}[\Delta f_\theta(t)\Delta\eta_{\theta'}^q(t)]^2}{\mathbb{E}[\Delta f_\theta(t)^2]\mathbb{E}[\Delta\eta_{\theta'}^q(t)^2]} = (\text{diag}(\sigma_A)^{-1}R)_{\theta\theta'}^2 Y_{\theta'}^2.\quad (52)$$

Figure 10 shows that the correlation between the forward rate and its generating white noise η^q exhibits vertical stripes related to the liquidity of the products considered. This is an effect of differences in the share Y_θ of the volatility explained by each white noise η_θ . However, the model cannot correct for the decreasing volatility of the noise field A , as shown by the lower R-squared in the top right of the matrix in Fig. 10. We would have obtained similar results in the BBDL

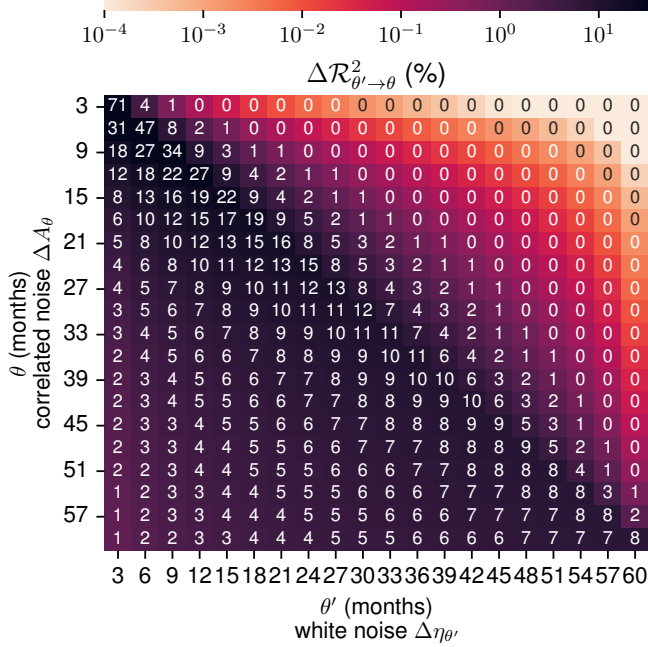


FIG. 9: Theoretical additional R-squared from regressing $\Delta A_\theta(t)$ on $\Delta\eta_{\theta'}(t)$ and $\Delta\eta_\theta(t)$ instead of solely $\Delta\eta_\theta(t)$, according to Eq. (15). The parameter κ is calibrated on forward rate correlations for the period 2021 – 2023 (i.e., $\kappa = 1.3$).

model, although it would require inserting a rotation factor $O_{\text{sym}}^2(\text{diag}(\sigma_A)^{-1}R\text{diag}(Y), I)$ into Eq. (52). As shown in the following section, this rotation also creates horizontal stripes that correspond to the symmetrization of the cross-impact matrix.

c. Responses of the forward rate to the order flow. In the BBDLS model, the additional R-squared from regressing $\Delta f_\theta(t)$ on $\Delta q_{\theta'}(t)$ and $\Delta q_\theta(t)$ instead of solely $\Delta q_\theta(t)$ is given by

$$\Delta\mathcal{R}_{\theta' \rightarrow \theta}^{2, \text{BBDLS}} = \lambda_{\theta\theta'}^2 \omega_{\theta'}^2 + 2\rho_{\theta\theta'}^q \lambda_{\theta\theta} \lambda_{\theta\theta'} \omega_\theta \omega_{\theta'}, \quad (53)$$

where $\lambda = \text{diag}(\sigma_A)^{-1}R\text{diag}(Y)O_{\text{sym}}\Omega^{-1/2}$ is 2×2 normalized cross-impact matrix in the BBDLS model. More precisely, the matrix $\text{diag}(\sigma_A)^{-1}R\text{diag}(Y)$ is given by the model of dimension n restricted to Futures contracts of tenor θ and θ' . The matrix $\Omega^{-1/2}$ is defined from a matrix Ω restricted to two Futures contracts of tenor θ and θ' .

Figure 11 shows that these additional R-squares exhibit vertical stripes related to the liquidity of the products considered. Although we reproduce the order of magnitude of the empirical measures (see Fig. 7), we do not precisely match the observed R-squared. In fact, we only have one parameter $Y_{\theta'}$ per column to correct the asymmetric shape of the correlation between ΔA and $\Delta\eta$

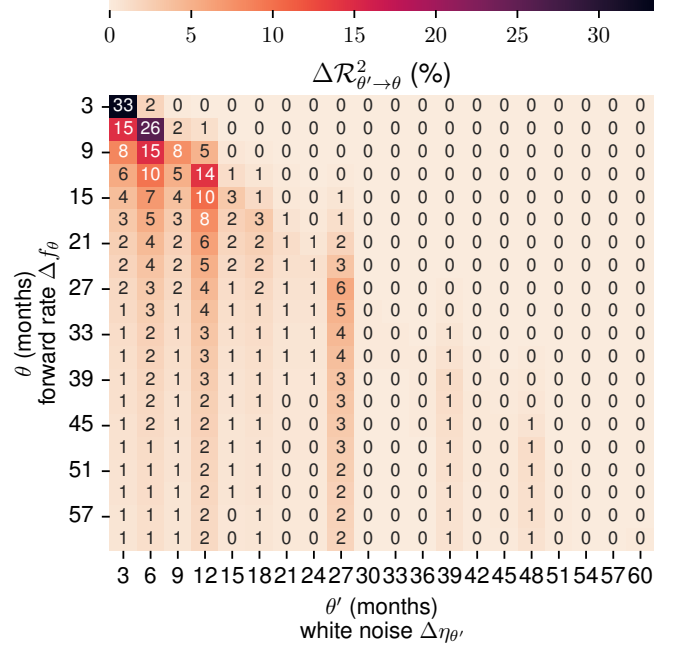


FIG. 10: Theoretical additional R-squared from regressing $\Delta f_\theta(t)$ on $\Delta\eta_{\theta'}^q(t)$ and $\Delta\eta_\theta^q(t)$ instead of solely $\Delta\eta_\theta^q(t)$. The parameter κ is calibrated on forward rate correlations for the period 2021 – 2023 (i.e., $\kappa = 1.3$) and Y is calibrated on the same period using the BBDLW model.

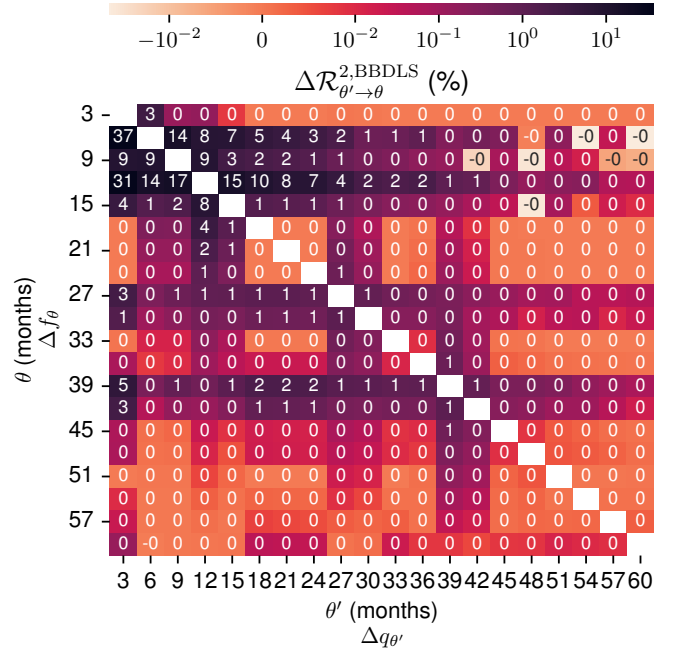


FIG. 11: Theoretical additional R-squared from regressing $\Delta f_\theta(t)$ on $\Delta q_{\theta'}(t)$ and $\Delta q_\theta(t)$ instead of solely $\Delta q_\theta(t)$. The parameter κ is calibrated on forward rate correlations for the period 2021 – 2023 (i.e., $\kappa = 1.3$) and Y is calibrated on the same period using the BBDLS model.

in Fig. 9. Thus, while the price-volume correlation depends on the respective liquidity of the considered asset pair (Le Coz *et al.*, 2024), in our model, it depends only on the explanatory asset. For a given order flow θ , we optimize the average Y_θ that best matches the liquidity of all assets.

Furthermore, in contrast with the empirical results, we observe that the BBDLS model generates horizontal stripes in the additional pairwise R-squared values (see Fig. 11). This occurs because of the symmetry of the cross-impact matrix imposed by the absence of arbitrage. As mentioned previously, the spatial correlation of the order flow is low (see Fig. 1), rendering the second term in Eq. (53) negligible. Consequently, pairwise R-squared values are primarily influenced by the term $\lambda_{\theta\theta}^2 \omega_{\theta'}^2$. We have seen that in the Kyle model, the liquidity $\omega_{\theta'}^2$ does not alter the price-volume correlation, so the R-squared values in Fig. 11 can be approximated by the product YY^\top , which is symmetric.

VII. CONCLUSION

Let us start by summarizing what we have achieved. First, we have shown that the BBDL model (Le Coz and Bouchaud, 2024) is consistent with the well-documented temporal autocorrelation of forward rates at short time scales. It appears that the time scale τ at which spatial correlations among asset prices emerge (Epps, 1979) is also the point where temporal correlations begin to dissipate. Therefore, this framework describes how the spatial and temporal correlation structure of prices evolves across time scales.

Most importantly, we have proposed a new interpretation of the BBDL model (Le Coz and Bouchaud, 2024) in which high-frequency shocks are identified to trades. The latter, which exhibit low spatial correlations, affect each point of the interest rate curve independently on the smallest time scale. The spatial correlation structure of prices emerges from market participants reacting to these independent trades and external shocks, such as news events, that simultaneously affect multiple points along the yield curve. These participants then propagate the impact of these shocks across other maturities through a self-referential mechanism, as described by Le Coz and Bouchaud (2024).

Consequently, this model can be interpreted as a cross-impact model, linking order flows to price movements. A key feature is that only the surprise component of trades influences prices, similarly to a propagator model. To address the challenge of temporal independence, we calibrate the model at a daily time scale, where trades show low autocorrelation. Using this approach, we can match or exceed the precision of the multivariate Kyle model in fitting price moves to order flows, but with far fewer parameters ($n + 1$ compared to $\frac{n(n-1)}{2}$). Further-

more, unlike the Kyle model, this framework accounts for liquidity-dependent correlations between the forward rate of one maturity and the order flow of another.

A promising direction for future research is to explore the micro-level mechanisms that connect liquidity with price-volume correlations. This would likely involve the development of a multidimensional model of the limit order book, shedding light on liquidity dynamics across different assets and maturities.

VIII. ACKNOWLEDGMENTS

We express our gratitude to Jean-Philippe Bouchaud and Damien Challet, who contributed to our research through fruitful discussions. We also thank Bertrand Hassani and the ANRT (CIFRE number 2021/0902) for providing us with the opportunity to conduct this research at Quant AI Lab. We extend our appreciation to Medhi Tomas for his assistance in designing the temporal and spatial decomposition of the order flow.

This research was carried out within the Econophysics & Complex Systems Research Chair, under the aegis of the Fondation du Risque, the Fondation de l'École polytechnique, the École polytechnique, and Capital Fund Management.

REFERENCES

- V. Le Coz and J.-P. Bouchaud, Revisiting Elastic String Models of Forward Interest Rates (2024).
- J. Hull, *Options, Futures, and Other Derivatives*, tenth edition ed. (Pearson, Chennai, 2018).
- D. Brigo and F. Mercurio, *Interest Rate Models, Theory and Practice: With Smile, Inflation and Credit*, 2nd ed., Springer Finance (Springer, Berlin, 2006).
- B. Baaquie and J.-P. Bouchaud, *Wilmott Magazine*, 2 (2004).
- T. W. Epps, *Journal of the American Statistical Association* **74**, 291 (1979).
- V. Le Coz, I. Mastromatteo, D. Challet, and M. Benzaquen, *Quantitative Finance* **24**, 265 (2024).
- D. Heath, R. Jarrow, and A. Morton, *Econometrica* **60**, 77 (1992).
- D. P. Kennedy, *Mathematical Finance* **4**, 247 (1994).
- D. P. Kennedy, *Mathematical Finance* **7**, 107 (1997).
- R. S. Goldstein, *Review of Financial Studies* **13**, 365 (2000).
- P. Santa-Clara and D. Sornette, *Review of Financial Studies* **14**, 149 (2001).
- B. E. Baaquie, *Physical Review E* **64**, 016121 (2001).
- B. E. Baaquie, *Physical Review E* **65**, 056122 (2002).
- B. E. Baaquie, *Quantum Finance: Path Integrals and Hamiltonians for Options and Interest Rates*, 1st ed. (Cambridge University Press, Cambridge, 2004).
- R. Cont, *International Journal of Theoretical and Applied Finance* **08**, 357 (2005).
- A. Bueno-Guerrero, M. Moreno, and J. F. Navas, *Physica A: Statistical Mechanics and its Applications* **433**, 229 (2015).
- A. Bueno-Guerrero, M. Moreno, and J. F. Navas, *Physica A: Statistical Mechanics and its Applications* **461**, 217 (2016).

- A. Bueno-Guerrero, M. Moreno, and J. F. Navas, *Physica A: Statistical Mechanics and its Applications* **559**, 125103 (2020).
- A. Bueno-Guerrero, M. Moreno, and J. F. Navas, *Quantitative Finance* **22**, 197 (2022).
- B. E. Baaquie, *Physical Review E* **75**, 016703 (2007).
- B. E. Baaquie, *Physical Review E* **80**, 046119 (2009).
- B. E. Baaquie, *Physica A: Statistical Mechanics and its Applications* **389**, 296 (2010).
- B. E. Baaquie, *Quantum Field Theory for Economics and Finance* (Cambridge University Press, Cambridge, United Kingdom, 2018).
- B. E. Baaquie and P. Tang, *Physica A: Statistical Mechanics and its Applications* **391**, 1287 (2012).
- B. E. Baaquie and C. Liang, *Physical Review E* **75**, 016704 (2007).
- T. L. Wu and S. Xu, *Journal of Futures Markets* **34**, 580 (2014).
- J.-P. Bouchaud, N. Sagna, R. Cont, N. El-Karoui, and M. Potters, *Applied Mathematical Finance* **6**, 209 (1999).
- A. S. Kyle, *Econometrica* **53**, 1315 (1985).
- J.-P. Bouchaud, J. Bonart, J. Donier, and M. Gould, *Trades, Quotes and Prices: Financial Markets Under the Microscope* (Cambridge University Press, Cambridge, UK ; New York, 2018).
- J.-P. Bouchaud, Y. Gefen, M. Potters, and M. Wyart, *Quantitative Finance* **4**, 176 (2004).
- F. Lillo and J. D. Farmer, *Studies in Nonlinear Dynamics & Econometrics* **8**, 10.2202/1558-3708.1226 (2004).
- J.-P. Bouchaud, J. D. Farmer, and F. Lillo, in *Handbook of Financial Markets: Dynamics and Evolution*, Handbooks in Finance, edited by T. Hens and K. R. Schenk-Hoppé (North-Holland, San Diego, 2009) pp. 57–160.
- R. Yamamoto and B. LeBaron, *The European Physical Journal B* **73**, 51 (2010).
- B. Tóth, I. Palit, F. Lillo, and J. D. Farmer, *Journal of Economic Dynamics and Control* **51**, 218 (2015).
- J.-P. Bouchaud, J. Kockelkoren, and M. Potters, *Quantitative Finance* **6**, 115 (2006).
- C. Hopman, *Quantitative Finance* **7**, 37 (2007).
- J.-P. Bouchaud, J. D. Farmer, and F. Lillo, in *Handbook of Financial Markets: Dynamics and Evolution* (arXiv, 2009).
- J. Gatheral, *Quantitative Finance* **10**, 749 (2010).
- J. Gatheral and A. Schied, in *Handbook on Systemic Risk*, edited by J.-P. Fouque and J. A. Langsam (Cambridge University Press, 2013) 1st ed., pp. 579–602.
- A. Alfonsi, F. Klöck, and A. Schied, *Mathematics of Operations Research* **41**, 914 (2016).
- N. Gârleanu and L. H. Pedersen, *Journal of Economic Theory* **165**, 487 (2016).
- B. Tóth, Z. Eisler, and J.-P. Bouchaud, *Market Microstructure and Liquidity* **03**, 1850002 (2017).
- D. E. Taranto, G. Bormetti, J.-P. Bouchaud, F. Lillo, and B. Tóth, *Quantitative Finance* **18**, 903 (2018).
- I. Ekren and J. Muhle-Karbe, *Mathematical Finance* **29**, 1066 (2019).
- J. P. Bouchaud, *Price Impact* (2009), arXiv:0903.2428 [q-fin].
- M. Benzaquen, I. Mastromatteo, Z. Eisler, and J.-P. Bouchaud, *Journal of Statistical Mechanics: Theory and Experiment* **2017**, 023406 (2017).
- M. Schneider and F. Lillo, *Quantitative Finance* **19**, 137 (2019).
- J. Hasbrouck and D. J. Seppi, *Journal of Financial Economics* **59**, 383 (2001).
- T. Chordia, A. Subrahmanyam, and V. Anshuman, *Journal of Financial Economics* **59**, 3 (2001).
- M. D. D. Evans and R. K. Lyons, *Why Order Flow Explains Exchange Rates*, Tech. Rep. (University of California, 2001).
- J. Harford and A. Kaul, *Journal of Financial and Quantitative Analysis* **40**, 29 (2005).
- P. Pasquariello and C. Vega, *Review of Financial Studies* **20**, 1975 (2007).
- S. C. Andrade, C. Chang, and M. S. Seasholes, *Journal of Financial Economics* **88**, 406 (2008).
- H. E. Tookes, *The Journal of Finance* **63**, 379 (2008).
- P. Pasquariello and C. Vega, *Review of Finance* **19**, 229 (2015).
- S. Wang and T. Guhr, *Market Microstructure and Liquidity* **03**, 1850009 (2017).
- M. Tomas, I. Mastromatteo, and M. Benzaquen, *Cross impact in derivative markets* (2022a), arXiv:2102.02834 [q-fin].
- M. Tomas, I. Mastromatteo, and M. Benzaquen, *Quantitative Finance* **22**, 1017 (2022b).
- D. Brigo, F. Graceffa, and E. Neuman, *Quantitative Finance* **22**, 171 (2022).
- V. Plerou, P. Gopikrishnan, B. Rosenow, L. A. Amaral, and H. Stanley, *Physica A: Statistical Mechanics and its Applications* **279**, 443 (2000).
- R. Cont, *Quantitative Finance* **1**, 223 (2001).
- S. Elomari-Kessab, G. Maitrier, J. Bonart, and J.-P. Bouchaud, *Disentangling the Joint Dynamics of Prices & Order Flow* (2024).
- M. Benzaquen, J. Donier, and J.-P. Bouchaud, *Market Microstructure and Liquidity* **02**, 1650009 (2016).
- L. C. G. del Molino, I. Mastromatteo, M. Benzaquen, and J.-P. Bouchaud, *SIAM Journal on Financial Mathematics* **11**, 327 (2020).

Appendix A: Notations

Table II summaries the notations used in this study.

Expression	Definition
n	The number of available SOFR Futures.
$\mathbf{M}_n(\mathbb{R})$	The set of real-valued square matrices of dimension n .
M^\top	The transpose of matrix M .
$\text{diag}(M)$	The vector in \mathbb{R}^n formed by the diagonal items of the matrix M .
$\text{diag}(v)$	The diagonal matrix whose components are the components (v_1, \dots, v_n) of the vector $v \in \mathbb{R}^n$.
$M^{1/2}$	A matrix such that $M^{1/2}(M^{1/2})^\top = M$.
\sqrt{M}	The unique positive semi-definite symmetric matrix such that $(\sqrt{M})^2 = M$.
$\Lambda(t)$	The cross-impact matrix at time t .
$\sigma(t)$	The vector of price variation volatility at time t .
$\omega(t)$	The vector of the signed order flow volatility at time t .
$\mathcal{R}^2(W)$	The W -weighted generalized R-squared.
$\Delta\mathcal{R}^2(W)$	The accuracy increase from the cross sectional model.
t	The current time.
T	The maturity.
$P(t, T)$	The price at time t of a zero-coupon bond maturing at T .
θ	The time-to-maturity or tenor.
$f_\theta(t)$	The value at time t of the instantaneous forward rate of tenor θ (discrete notation).
$f(t)$	The vector of forward rates at time t .
$\Delta q_\theta(t)$	The net market order flow traded during the time window $[t, t + \Delta t]$.
$\Delta q(t)$	The vector of the net traded order flows during the time window $[t, t + \Delta t]$.
$A_\theta(t)$	The driftless correlated noise field.
$\eta_\theta(\cdot)$	The discrete white noise of tenor θ .
$\sigma_\theta(t)$	The volatility at time t of the infinitesimal variation of the instantaneous forward rate of time-to-maturity θ .
μ	The line tension parameter.
ψ	The psychological time parameter.
κ	Unique a-dimensional parameter in the BBDL model, defined as the product $\mu \times \psi$.
τ	The time scale for the emergence of correlations.
Δt	The temporal duration of a day.
$\mathbb{E}[\cdot]$	The unconditional expectancy.
$\langle \cdot \rangle(t)$	The empirical average operator over the interval $[t - \Delta t, t]$.
$\hat{x}(t)$	The estimator of x at time t .
$\eta_\theta(\cdot)$	The discrete white noise of tenor θ .
$\delta(\cdot)$	The Dirac delta function.
$\rho(x, y)$	The linear Pearson correlation matrix between the random vector x and y .
$\delta_{\theta\theta'}$	The Kronecker delta.
I_k	A matrix with ones only on the k -th diagonal above the main diagonal.
I	The identity matrix.
\mathcal{J}	A diagonal matrix whose first entry is 2 while all the other entries are ones.
$\mathcal{L}_d[\cdot]$	The discrete linear differential operator on space.
\mathcal{M}	The discrete non-linear differential operator on space, using matrix notations.
$L_d[\cdot]$	The Fourier transform of the discrete linear differential operator on space.
$G_{\theta\theta'}(\cdot)$	Green function or <i>propagator</i> of Eq. (4)
N	The number of days in a 3-year period of our sample.
$H(\cdot)$	The Heaviside function.
$\mathcal{F}[f]$	The Fourier transform of the function of time f .

TABLE II: Notations

Appendix B: Responses to the white noise for $\psi \gg 1$

1. Covariance

We derive the covariance between $\Delta A_\theta(t)$ and $\Delta \eta_{\theta'}(t)$ in the limit $\psi \gg 1$:

$$\begin{aligned}
& \mathbb{E}[\Delta A_\theta(t) \Delta \eta_{\theta'}(t)] \\
&= \int_{t-\Delta t}^t du \int_{t-\Delta t}^t dv \mathbb{E}[A_\theta(u) \eta_{\theta'}(v)] \\
&= \frac{1}{\tau} \int_{t-\Delta t}^t du \int_{t-\Delta t}^u dv G_{\theta, \theta'}(u-v) \\
&= \frac{1}{2\pi\tau} \int_{-\pi}^{\pi} d\xi \left(e^{i\xi(\theta-\theta')} + e^{i\xi(\theta+\theta')} \right) \\
&\quad \int_{t-\Delta t}^t du \int_{t'-\Delta t}^u dv e^{-\frac{L_d(\xi)}{\tau}(u-v)} \\
&= \frac{1}{2\pi} \int_{-\pi}^{\pi} d\xi \frac{e^{i\xi(\theta-\theta')} + e^{i\xi(\theta+\theta')}}{L_d(\xi)} \\
&\quad \int_{t-\Delta t}^t du \left(1 - e^{-\frac{L_d(\xi)}{\tau}(u-t+\Delta t)} \right) \\
&\xrightarrow{\tau \rightarrow 0} \Delta t (\mathcal{D}_1)_{\theta\theta'}. \tag{B1}
\end{aligned}$$

2. Correlation

Using Eq. (B1), we obtain the correlation between $\Delta A_\theta(t)$ and $\Delta \eta_{\theta'}(t)$:

$$\frac{\mathbb{E}[\Delta A_\theta(t) \Delta \eta_{\theta'}(t)]}{\sqrt{\mathbb{E}[\Delta A_\theta(t)^2] \mathbb{E}[\Delta \eta_{\theta'}(t)^2]}} = \frac{(\mathcal{D}_1)_{\theta\theta'}}{\sqrt{(\mathcal{D}_2)_{\theta\theta}}}. \tag{B2}$$

We can show that Eq. (B2) is well defined. For this purpose, we define the usual inner product (f, g) between two integrable real-valued functions f and g on $[0, \pi]$ by:

$$(f, g) = \frac{1}{\pi} \int_0^\pi d\xi f(\xi) g(\xi). \tag{B3}$$

For $(\theta, \theta') \in [[1, n]]^2$, having noted that $\frac{2}{\pi} \int_0^\pi d\xi \cos^2 \xi \theta = 1$, we have:

$$(\mathcal{D}_1)_{\theta\theta'} = \left(\frac{\sqrt{2} \cos \xi \theta}{L_d(\xi)}, \sqrt{2} \cos \xi \theta' \right), \tag{B4}$$

$$(\mathcal{D}_2)_{\theta\theta} = \left(\frac{\sqrt{2} \cos \xi \theta}{L_d(\xi)}, \frac{\sqrt{2} \cos \xi \theta}{L_d(\xi)} \right) \left(\sqrt{2} \cos \xi \theta', \sqrt{2} \cos \xi \theta' \right). \tag{B5}$$

Thus, Cauchy-Schwarz's inequality ensures that

$$-1 \leq \frac{(\mathcal{D}_1)_{\theta\theta'}}{\sqrt{(\mathcal{D}_2)_{\theta\theta}}} \leq 1. \tag{B6}$$

Appendix C: Responses to the white noise for $\psi \ll 1$

1. Covariance

We derive the covariance between $\Delta A_\theta(t)$ and $\Delta \eta_{\theta'}(t)$ in the limit $\psi \ll 1$:

$$\begin{aligned}
& \mathbb{E} [\Delta A(t) \Delta \eta(t)^\top] \\
&= \int_{t-\Delta t}^t du \int_{t-\Delta t}^t dv \mathbb{E} [A(u) \eta(v)^\top] \\
&= \frac{1}{\tau} \int_{t-\Delta t}^t du \int_{t-\Delta t}^u dv e^{-\frac{u-v}{\tau} \mathcal{M}} \mathcal{J} \\
&= \int_{t-\Delta t}^t du \mathcal{M}^{-1} \left(1 - e^{-\frac{u-t+\Delta t}{\tau} \mathcal{M}} \right) \mathcal{J} \\
&\xrightarrow{\tau \rightarrow 0} \Delta t \mathcal{M}^{-1} J. \tag{C1}
\end{aligned}$$

2. Correlation

Using Eq. (C1), we obtain the correlation between $\Delta A_\theta(t)$ and $\Delta \eta_{\theta'}(t)$:

$$\frac{\mathbb{E} [\Delta A_\theta(t) \Delta \eta_{\theta'}(t)]}{\sqrt{\mathbb{E} [\Delta A_\theta(t)^2] \mathbb{E} [\Delta \eta_{\theta'}(t)^2]}} = \frac{(\mathcal{M}^{-1} \mathcal{J})_{\theta\theta'}}{\sqrt{(\mathcal{M}^{-1} \mathcal{J}^2 (\mathcal{M}^{-1})^\top)_{\theta\theta}}}, \tag{C2}$$

which is clearly well defined.

Appendix D: Order flow decomposition

Let η^q be a white noise vector such that $\mathbb{E} [\eta_\theta^q(t) \eta_{\theta'}^q(t')] = \delta_{\theta\theta'} \delta(t-t')$. We decompose the trading flow across time and space into the cumulative sum of η^q and a kernel K :

$$\frac{dq}{dt}(t) = \int_{-\infty}^t dt' K(t, t') O^\top \eta^q(t'), \tag{D1}$$

where O is an orthogonal matrix and the kernel $K(u, u') \in \mathbf{M}_n(\mathbb{R})$ is such that the lagged variance-covariance matrix $\Omega(t, t')$ of the infinitesimal order flow imbalance reads

$$\begin{aligned}
\Omega(t, t') &:= \mathbb{E} \left[\frac{dq}{dt}(t) \frac{dq}{dt}^\top(t') \right] \\
&= \int_{-\infty}^t du \int_{-\infty}^{t'} dv K(t, u) O^\top \mathbb{E} [\eta^q(u) \eta^q(v)^\top] \\
&\hspace{15em} O K^\top(t', v) \\
&= \int_{-\infty}^{\min(t, t')} du K(t, u) K^\top(t', u). \tag{D2}
\end{aligned}$$

We assume that the series of matrices $(K(t, t'))_{t \geq 0, t' \geq 0}$ can be written $K(t-t')_{t-t' \geq 0}$. Under this assumption,

the lagged variance-covariance matrix $\Omega(t, t')$ is stationary and can be written as a function of the lag $\ell = t - t'$:

$$\begin{aligned}
\Omega(t, t-\ell) &= \int_{\mathbb{R}} du K(t-u) K^\top(t-\ell-u) \\
&= \int_{\mathbb{R}} du' K(u') K^\top(u'-\ell). \tag{D3}
\end{aligned}$$

The Fourier transform over the lag ℓ of Eq. (D3) reads

$$\mathcal{F}[\Omega](m) = \mathcal{F}[K](m) \{ \mathcal{F}[K](m) \}^\top, \tag{D4}$$

where $\mathcal{F}[K]$ and $\mathcal{F}[\Omega]$ are the Fourier transform of $\ell \rightarrow K(\ell)$ and $\ell \rightarrow \Omega(\ell)$. Thus, Eq. (D1) is verified if and only if, each matrix $\mathcal{F}[K](m)$ is a decomposition of $\mathcal{F}[\Omega](m)$:

$$\mathcal{F}[K](m) = \{ \mathcal{F}[\Omega](m) \}^{1/2}. \tag{D5}$$

For example, we can build numerically each $\mathcal{F}[K](m)$ as the Cholesky decomposition of $\mathcal{F}[\Omega](m)$.

Still assuming stationarity, the definition of $q(t)$ in Eq. (D1) reads as the convolution product of K and η . The Fourier transform over time of Eq. (D1) reads in matrix notations

$$\mathcal{F} \left[\frac{dq}{dt} \right] (m) = \mathcal{F}[K](m) O^\top \mathcal{F}[\eta^q](m). \tag{D6}$$

Assuming the matrix $\hat{K}(m)$ is invertible one can write Eq. (D6) as

$$\mathcal{F}[\eta^q](m) = O \{ \mathcal{F}[K](m) \}^{-1} \mathcal{F} \left[\frac{dq}{dt} \right] (m). \tag{D7}$$

Hence, one can also write the white noise η^q as the convolution product:

$$\eta^q(t) = O \int_{-\infty}^t dt' J(t-t') \frac{dq}{dt}(t'), \tag{D8}$$

where the function $u \mapsto J(u)$, valued in $\mathbf{M}_n(\mathbb{R})$, is the inverse Fourier transform of $m \mapsto \{ \mathcal{F}[K](m) \}^{-1}$.

Appendix E: Large-bin approximation

In this section, we denote by $\bar{x}_{\Delta t}$ the observed empirical average over the time interval $[t-\Delta t, t]$ of the random process $x(t)$ (i.e., its moving average):

$$\bar{x}_{\Delta t}(t) := \frac{1}{\Delta t} \int_{t-\Delta t}^t dt' x(t'). \tag{E1}$$

We aim to approximate $\Delta A_\theta(t)$ as a function of coarse-grained variables $\Delta \eta$ defined over intervals of finite width Δt . For this purpose, we decompose the white noise $\eta(t')$ as the sum of its moving average and its fluctuations around this mean. Formally, we write

$$\eta(t') = \bar{\eta}_{\Delta t}(t) + \eta(t') - \bar{\eta}_{\Delta t}(t). \tag{E2}$$

The independence and stationarity of η across time ensures that $\bar{\eta}_{\Delta t}(t)$ is uncorrelated with $\eta(t') - \bar{\eta}_{\Delta t}(t)$:

$$\begin{aligned} & \mathbb{E} [\bar{\eta}_{\Delta t}(t) (\eta(t') - \bar{\eta}_{\Delta t}(t))] \\ &= \frac{1}{\Delta t} \int_{t-\Delta t}^t dt'' \mathbb{E} [\eta(t') \eta(t'')] \\ & \quad - \frac{1}{(\Delta t)^2} \iint_{t-\Delta t}^t dt'' dt''' \mathbb{E} [\eta(t'') \eta(t''')] \\ &= \frac{1}{\Delta t} - \frac{1}{\Delta t} = 0. \end{aligned} \quad (\text{E3})$$

In fact, the continuous-time hypothesis, which is related to the Gaussianity of the Langevin noise η , ensures the independence between $\bar{\eta}_{\Delta t}(t)$ and $\eta(t') - \bar{\eta}_{\Delta t}(t)$ (although only an absence of correlation is needed here). It is worth mentioning that this result can also be derived by observing that the process $\int_0^t dt' \eta(t') - \int_0^t dt' \bar{\eta}_{\Delta t}(t')$ is a Brownian bridge.

We now define the matrix $R^\tau(t)$ by

$$R^\tau(t) = \frac{1}{\tau} \int_{-\infty}^t dt' G(t-t'). \quad (\text{E4})$$

Correlations among assets appear at a time scale $\tau \ll \Delta t$ (Le Coz and Bouchaud, 2024; Epps, 1979) and the time decay of G is very strong: $G_{\theta\theta'}(5\tau)/G_{\theta\theta'}(0) \approx 10^{-3}$ for typical values of $\kappa \approx 1$. Hence, we can approximate $R^\tau(t)$ by

$$R^\tau(t) \approx \frac{1}{\tau} \int_{t-\Delta t}^t dt' G(t-t'). \quad (\text{E5})$$

Substituting η by Eq. (E2) in the definition (6) of the noise field $A(t)$ yields

$$A(t) = R^\tau(t) \bar{\eta}_{\Delta t}(t) + \epsilon^\tau(t), \quad (\text{E6})$$

where $\epsilon^\tau(t) = \frac{1}{\tau} \int_{t-\Delta t}^t dt' G(t-t') (\eta(t') - \bar{\eta}_{\Delta t}(t))$ is a noise independent from $\bar{\eta}_{\Delta t}(t)$. Importantly, ϵ^τ has no temporal correlation but has a spatial structure allowing to retrieve the spatial correlations of $A(t)$. The integration of Eq. (E6) over the interval $[t-\Delta t, t]$ yields an affine relationship between ΔA the sum of A over one day, and the empirical daily means $\bar{\eta}_{\Delta t}(t)$:

$$\Delta A(t) = \left(\int_{t-\Delta t}^t dt' R^\tau(t') \right) \bar{\eta}_{\Delta t}(t) + \int_{t-\Delta t}^t dt' \epsilon^\tau(t'). \quad (\text{E7})$$

One can substitute η with η^q or η^\top and A with A^q or A^\top respectively in Eq. (E7). Thus, having noted that $\langle \Delta A^\perp(t) \Delta \eta^q(t) \rangle = 0$, one can relate forward rate daily increments to the empirical daily means of the martingale

component of the order flow:

$$\begin{aligned} \Delta f(t) &= \\ & \text{diag}(\sigma) \text{diag}(\sigma_A)^{-1} \left(\int_{t-\Delta t}^t dt' R^\tau(t') \right) \\ & \quad \text{diag}(Y) O \Omega^{-1/2} \frac{d\tilde{q}}{dt \Delta t}(t) + \mathcal{E}^\tau(t), \end{aligned} \quad (\text{E8})$$

where the residual noise $\mathcal{E}^\tau(t)$ is independent from $\frac{d\tilde{q}}{dt \Delta t}(t)$. Indeed, $\mathcal{E}^\tau(t)$ reads

$$\begin{aligned} \mathcal{E}^\tau(t) &= \\ & \text{diag}(\sigma) \text{diag}(\sigma_A)^{-1} \left(\int_{t-\Delta t}^t dt' R^\tau(t') \right) \text{diag}(Y^\perp) \bar{\eta}_{\Delta t}^\perp(t) \\ & \quad + \text{diag}(\sigma_A)^{-1} \int_{t-\Delta t}^t dt' \epsilon^\tau(t'). \end{aligned} \quad (\text{E9})$$

Moreover, by definition of the empirical mean, we have

$$\frac{d\tilde{q}}{dt \Delta t}(t) = \frac{1}{\Delta t} \int_{t-\Delta t}^t dt' \frac{d\tilde{q}}{dt'}(t') = \frac{\Delta \tilde{q}(t)}{\Delta t}. \quad (\text{E10})$$

We denote $\widehat{\Delta f}$ the conditional expectancy of the forward rates increments Δf with respect to the martingale component of the order flows $\Delta \tilde{q}(t)$:

$$\widehat{\Delta f}(t) := \mathbb{E} [\Delta f(t) | \Delta \tilde{q}(t)]. \quad (\text{E11})$$

Taking the conditional expectancy of Eq. (E8) yields

$$\begin{aligned} \widehat{\Delta f}(t) &= \\ & \text{diag}(\sigma) \text{diag}(\sigma_A)^{-1} \left(\int_{t-\Delta t}^t dt' R^\tau(t') \right) \text{diag}(Y) O \Omega^{-1/2} \frac{\Delta \tilde{q}(t)}{\Delta t}. \end{aligned} \quad (\text{E12})$$

One can choose τ arbitrarily small in the expression of $R^\tau(t)$. In the limit $\tau \ll 1$ we have

$$R^\tau(t) \xrightarrow{\tau \rightarrow 0} R. \quad (\text{E13})$$

Thus, in this limit, Eq. (E12) reads

$$\widehat{\Delta f}(t) = \text{diag}(\sigma) \text{diag}(\sigma_A)^{-1} R \text{diag}(Y) O \Omega^{-1/2} \Delta \tilde{q}(t). \quad (\text{E14})$$

In this model, the residual noise \mathcal{E} in Eq. (33) can be seen as the limit for small τ of $\mathcal{E}^\tau(t)$.

Appendix F: Response to order flows

In this appendix we show that

$$\begin{aligned} & \mathbb{E} [\Delta f(t) \Delta q^\top(t)] \mathbb{E} [\Delta q(t) \Delta q^\top(t)]^{-1} \\ &= \text{diag}(\sigma) \text{diag}(\sigma_A)^{-1} R \text{diag}(Y) O \Omega^{-1/2}. \end{aligned} \quad (\text{F1})$$

For this purpose we first derive the expression of the covariance $\mathbb{E} [\Delta f(t) \Delta q(t)^\top]$. We also show that the correlation between the forward rates and the order flows is well defined.

1. Computation of the covariance matrix

In this section we derive the expression of the covariance between forward rates and order flows.

We define the accumulated trading flows over the period $[t, t + \Delta t]$, representing a trading day, as

$$\Delta q(t) = \int_{t-\Delta t}^t dt' \frac{dq}{dt}(t'). \quad (\text{F2})$$

The equal-time covariance between $\Delta A^q(t)$ and $\Delta q(t)$ is

$$\begin{aligned} \mathbb{E} [\Delta A^q(t) \Delta q^\top(t)] &= \iint_{t-\Delta t}^t dudv \int_{-\infty}^v dv' \\ &\mathbb{E} [A^q(u) \eta^q(v')^\top] OK^\top(v - v'). \end{aligned} \quad (\text{F3})$$

Eq. (26) and (6) imply that $\mathbb{E} [A^q(u) \eta^q(v')^\top] = \frac{1}{\tau} G(u - v')$ $\text{diag}(Y)$, so the previous expression becomes

$$\begin{aligned} \mathbb{E} [\Delta A^q(t) \Delta q^\top(t)] &= \frac{1}{\tau} \iint_{t-\Delta t}^t dudv \int_{-\infty}^v dv' G(u - v') \text{diag}(Y) OK^\top(v - v'). \end{aligned} \quad (\text{F4})$$

For $\tau \ll 1$, we have $\frac{1}{\tau} G(t - t') \rightarrow R\delta(t - t')$ (Le Coz and Bouchaud, 2024). It yields

$$\begin{aligned} \mathbb{E} [\Delta A^q(t) \Delta q(t)] &= R \text{diag}(Y) O \iint_{t-\Delta t}^t dudv K^\top(v - u) \\ &= \Delta t R \text{diag}(Y) O \int_0^{\Delta t} d\ell K^\top(\ell). \end{aligned} \quad (\text{F5})$$

Thus, the covariance between the forward rates and the order flows reads

$$\begin{aligned} \mathbb{E} [\Delta f(t) \Delta q^\top(t)] &= \Delta t \text{diag} \sigma \text{diag}(\sigma_A)^{-1} R \text{diag}(Y) O \int_0^{\Delta t} d\ell K^\top(\ell), \end{aligned} \quad (\text{F6})$$

having noted that $\mathbb{E} [\Delta A^\perp(t) \Delta q^\top(t)] = 0$.

2. Computation of the response matrix

We define the cross-impact matrix $\Lambda \in \mathbf{M}_n(\mathbb{R})$ as the matrix ensuring a linear relationship between forward rates increments and order flows, i.e.,

$$\Delta f(t) = \Lambda \Delta q(t) + \mathcal{E}(t), \quad (\text{F7})$$

where \mathcal{E} is a temporally uncorrelated noise independent from Δq . One can reformulate (F7) as

$$\mathbb{E} [\Delta f(t) \Delta q(t)^\top] = \Lambda \mathbb{E} [\Delta q(t) \Delta q(t)^\top]. \quad (\text{F8})$$

Yet, the variance covariance matrix of the daily trading flow imbalance reads

$$\begin{aligned} \mathbb{E} [\Delta q(t) \Delta q^\top(t)] &= \iint_{t-\Delta t}^t ds ds' \mathbb{E} \left[\frac{dq}{dt}(s) \frac{dq}{dt}^\top(s') \right] \\ &= \iint_{t-\Delta t}^t ds ds' \int_{-\infty}^{\min(s, s')} du K(s - u) K^\top(s' - u) \\ &= \Delta t \int_0^{\Delta t} dl \int_{\mathbb{R}} du K(u) K^\top(u - l). \end{aligned} \quad (\text{F9})$$

Hence, replacing the left-hand side in (F8) by its expression in (F6), we have

$$\begin{aligned} \text{diag} \sigma \text{diag}(\sigma_A)^{-1} R \text{diag}(Y) O \int_0^{\Delta t} d\ell K^\top(\ell) = \\ \Lambda \int_0^{\Delta t} d\ell K * K^\top(\ell). \end{aligned} \quad (\text{F10})$$

In the most general case, Eq. (F10) requires Λ to be time-dependent. Yet, assuming dq has no temporal correlation i.e., $K(u) = \delta(u) \Omega^{1/2}$, Eq. (F10) reads

$$\Lambda = \text{diag} \sigma \text{diag}(\sigma_A)^{-1} R \text{diag}(Y) O \Omega^{-1/2}, \quad (\text{F11})$$

where the equal-time variance-covariance matrix Ω is defined by $\Omega := \frac{\mathbb{E}[\Delta q(t) \Delta q^\top(t)]}{\Delta t}$.

Appendix G: Correlation between forward rates and flows

In this section, we demonstrate that the correlation between the forward rate of tenor θ and the martingale component of the order flow of tenor θ' , given by,

$$\rho(\Delta f_\theta(t), \Delta \tilde{q}_{\theta'}(t)) = \sum_{\theta''=1}^n \frac{R_{\theta\theta''}}{(\sigma_A)_\theta} Y_{\theta''} \frac{(\Omega^{1/2} O^\top)_{\theta'\theta''}}{\sqrt{\Omega_{\theta'\theta'}}}, \quad (\text{G1})$$

is well-defined. We assume $Y = 1$, the unit vector. In the case $\psi \ll 1$, $(\sigma_A)_\theta = \sqrt{(\mathcal{M}^{-1} \mathcal{J}^2 (\mathcal{M}^{-1})^\top)_{\theta\theta}}$ and $R_{\theta\theta'} = (\mathcal{M}^{-1} \mathcal{J})_{\theta\theta'}$. Equation (G1) is then the canonical inner product of two normalized vectors of \mathbb{R}^n . Thus, the correlation $\rho(\Delta f_\theta(t), \Delta \tilde{q}_{\theta'}(t))$ is well defined.

In the case $\psi \gg 1$, one can express the numerator and the denominator in Eq. (G1) using the inner product (B3) on the space of integrable real-valued functions on $[0, \pi]$. For $(\theta, \theta') \in \llbracket 1, n \rrbracket^2$, having noted that $(\sqrt{2} \cos \xi \theta, \sqrt{2} \cos \xi \theta') = \delta_{\theta\theta'}$, we have

$$\begin{aligned} \sum_{\theta''=1}^n (R)_{\theta\theta''} (\Omega^{1/2} O)_{\theta'\theta''} &= \sum_{\theta''=1}^n (\mathcal{D}_1)_{\theta\theta''} (\Omega^{1/2} O)_{\theta'\theta''} \\ &= \left(\frac{\sqrt{2} \cos \xi \theta}{L_d(\xi)}, \sqrt{2} \sum_{\theta''=1}^n \cos \xi \theta'' (\Omega^{1/2} O)_{\theta'\theta''} \right), \end{aligned} \quad (\text{G2})$$

and,

$$\begin{aligned}
(\sigma_A)_\theta \Omega_{\theta'\theta'} &= (\mathcal{D}_2)_{\theta\theta} \Omega_{\theta'\theta'} \\
&= \left(\frac{\sqrt{2} \cos \xi\theta}{L_d(\xi)}, \frac{\sqrt{2} \cos \xi\theta}{L_d(\xi)} \right) \times \\
&\quad \left(\sqrt{2} \sum_{\theta''=1}^n \cos \xi\theta'' (\Omega^{1/2}O)_{\theta'\theta''}, \sqrt{2} \sum_{\theta''=1}^n \cos \xi\theta'' (\Omega^{1/2}O)_{\theta'\theta''} \right).
\end{aligned} \tag{G3}$$

Thus, Cauchy-Schwarz's inequality ensures

$$-1 \leq \frac{\sum_{\theta''=1}^n (\mathcal{D}_1)_{\theta\theta''} (\Omega^{1/2}O)_{\theta'\theta''}}{\sqrt{(\mathcal{D}_2)_{\theta\theta} \Omega_{\theta'\theta'}}} \leq 1. \tag{G4}$$